Calcium Halophosphate Phosphors

I. Analysis of Emission Spectra[1]

KEITH H. BUTLER AND CHARLES W. JEROME

Sylvania Electric Products Incorporated, Salem, Massachusetts

ABSTRACT

The energy distribution of the emission spectra of a number of calcium halophosphate phosphors has been determined on a recording spectroradiometer. These emission curves have been broken down into component bands, each of which has a Gaussian distribution of energy against wave number. An attempt is made to assign the emission bands to specific energy levels of the excited ions and to interpret their changes in terms of crystal structure and location of the activator atoms.

In a paper (1) by one of the present authors it has been shown that the emission spectra of silicate phosphors with manganese activation, when plotted on a frequency scale, can be expressed as the sum of several Gaussian distribution curves. Two independent studies (2, 2a, 3) have confirmed the data on zinc beryllium silicate, not only in reference to the complexity of the manganese emission spectrum but also as to the location of the components. Previous workers (4, 5) have described the preparation of calcium halophosphates and outlined the characteristics of the emission spectrum in part, but have not analyzed the experimental results.

The same technique used for the silicates has been applied to the analysis of the emission spectra of the halophosphate phosphors, and although the emission is simpler than that of the silicate phosphors, it is found to consist of four or more Gaussian components —two of which are associated with the antimony activator and at least two with the manganese activator. Changes in composition vary the amplitude of all bands. Both the location and shape of the antimony bands are invariant with composition, while, in contrast, an increase in the chloride content shifts the position of the manganese bands toward lower frequency although their shape remains constant.

EXPERIMENTAL PROCEDURE

The phosphors were prepared by milling together the calcium phosphate and other raw materials in needed proportions for phosphor production. The blend was then fired in silica vessels for three hours at temperatures in the range 1000° to 1200°C and the phosphors of maximum brightness selected for further test. The ingredient proportions and the method of firing chosen were optimum for phosphors with a moderate amount of chloride. Somewhat modified compositions and changed firing methods gave higher brightness powders with very low chloride or high chloride, but the color of the emission was not affected by such changes, as the intensities of all emission bands were increased proportionately to overall brightness. It was decided, therefore, to use phosphors prepared in the same way for further work. The selected phosphors were ground in butyl acetate to suitable fineness, nitrocellulose lacquer added, and the milled suspension adjusted to give the correct coating thickness of the bulb. The coated bulbs were baked to remove the binder, electrodes sealed in, and the lamps exhausted on production equipment, with 20-watt lamps of the usual fluorescent type being made. The spectral energy distribution of the lamps was measured on a spectroradiometer, described in a recent paper (6), which plots automatically the relative emitted energy as a function of wavelength. The color parameters of the phosphor emission were computed for the I.C.I. color mixture diagram from the spectral energy distribution, using the selected ordinate method (7). The energy distribution curve was then replotted on a reciprocal wavelength scale and analyzed graphically for the amplitude, shape, and position of the component Gaussian emission bands.

RESULTS

Components of the Emission Bands of Halophosphates

The present paper covers a systematic analysis of the spectral energy curves of 45 phosphors, with the range of composition including 8 different ratios of fluoride to chloride at 6 manganese contents. Fig. 1 shows the spectral energy distribution of a typical halophosphate and its component Gaussian bands. The agreement between the envelope of the components and the observed data is good throughout most of the spectrum. Fig. 2 shows a typical set of curves as recorded by the radiometer, with the manganese content being varied, at a constant fluoride to

[1] Manuscript received April 4, 1950. This paper prepared for delivery before the Cleveland Meeting, April 19 to 22, 1950.

chloride ratio. Tables I to IV list the parameters $1/\lambda_0$, A and σ for each of the Gaussian bands as affected by the composition. Part of the data in these tables is also plotted in Fig. 3, 4, and 5. The composition values are given as atoms of the particular ion for each three atoms of phosphorus in the initial blend of raw materials. Our analyses of the phosphors indicate that considerable amounts of some of the ingredients are volatilized during the firing with the evaporation rates being different for different compositions and also dependent upon firing conditions. However, this will be the subject of a future paper when more complete information has been obtained.

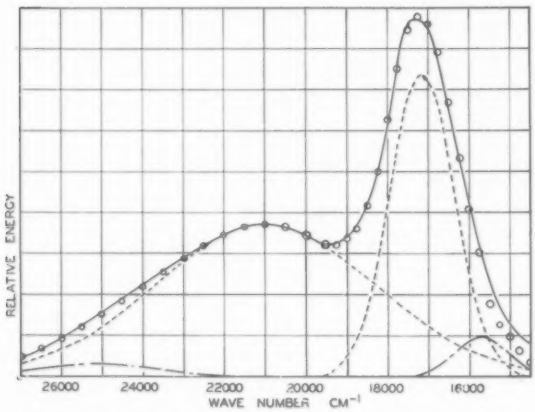

FIG. 1. Spectral energy distribution of a halophosphate with component Gaussian bands. Solid line—observed spectral energy distribution, broken lines—Gaussian bands, circles—envelope of Gaussian bands.

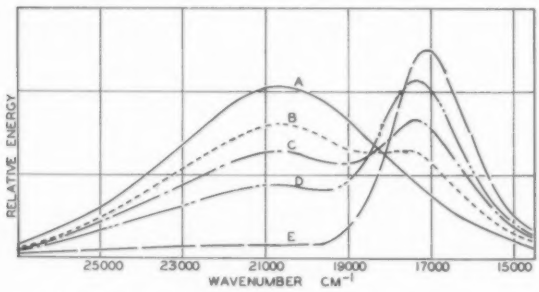

FIG. 2. Effect of manganese concentration on spectra energy distribution of halophosphates. A—0.000 gram atoms Mn per 3 gram atoms of P, B—0.025 gram atoms Mn per 3 gram atoms of P, C—0.050 gram atoms Mn per 3 gram atoms of P, D—0.100 gram atoms Mn per 3 gram atoms of P, E—0.400 gram atoms Mn per 3 gram atoms of P.

TABLE I. *Effect of composition on major Sb band*
$1/\lambda_0 = 20{,}500 \pm 500$ cm^{-1}, $\sigma = 2700$

% Cl	0 Mn	0.025	0.05	0.10	0.20	0.40
0	30.0	23.0	18.5	12.5	5.0	1.5
10	33.5	—	20.0	—	—	1.0
20	42.5	29.5	25.0	15.0	6.8	1.5
25	42.5	34.0	28.0	18.5	7.5	2.0
30	35.0	30.0	30.0	16.5	7.0	2.0
50	33.0	24.8	22.8	14.0	7.0	2.5
75	23.5	19.0	15.5	9.3	4.0	2.0
100	16.5	9.0	8.5	6.0	2.8	1.0

A study was made first of phosphors activated by antimony alone. This showed that two components were present in the antimony emission and that these were constant in shape and position, regardless of the chloride content, with the main band falling at 20,500 cm^{-1} (4870 Å) and the minor band at 25,225 cm^{-1} (3960 Å). However, the relative intensity changes with the ratio of fluoride to chloride. The major band goes through a maximum value as the chloride content increases, while the minor band

TABLE II. *Effect of composition on minor Sb band*
$1/\lambda_0 = 25{,}225$ cm$^{-1} \pm 500$, $\sigma = 1500$

% Cl	0 Mn	0.025	0.05	0.10	0.20	0.40
0	13.0	14.0	15.5	10.5	4.0	1.0
10	10.5	—	11.0	—	—	1.0
20	5.0	5.0	4.0	3.0	2.5	1.5
25	3.5	1.7	1.4	0.7	0.5	—
30	3.0	4.0	4.0	1.7	2.5	—
50	2.0	1.9	1.9	3.0	2.7	2.0
75	2.6	1.5	1.2	2.0	1.7	1.7
100	1.0	2.0	1.5	1.5	1.8	1.0

TABLE III. *Effect of composition on major Mn band*
$\sigma = 800$

% Cl	$1/\lambda_0$	Amplitude					
		Mn:0	0.025	0.05	0.10	0.20	0.40
0	17,550 ± 50	—	15.0	20.0	30.5	39.0	33.8
10	17,525 ± 225	—	—	21.5	—	—	34.8
20	17,330 ± 120	—	13.0	25.0	33.5	43.5	33.0
25	17,240 ± 40	—	11.8	23.0	36.0	37.0	50.0
30	17,110 ± 110	—	12.3	30.0	36.5	49.0	49.0
50	17,010 ± 110	—	11.0	22.0	33.0	45.0	40.0
75	16,940 ± 140	—	11.0	17.0	26.0	29.5	28.5
100	16,800 ± 300	—	9.5	15.5	23.0	28.0	17.5

TABLE IV. *Effect of composition on minor Mn band*
$\sigma = 650$

% Cl	$1/\lambda_0$	Amplitude					
		Mn:0	0.025	0.05	0.10	0.20	0.40
0	16,020 ± 65	—	2.5	4.0	5.5	6.0	6.5
10	16,125 ± 325	—	—	7.0	—	—	6.5
20	15,480 ± 190	—	1.5	2.5	7.0	5.0	4.5
25	15,690 ± 75	—	3.0	4.8	8.0	10.5	11.0
30	15,610 ± 150	—	3.0	8.0	10.0	11.0	10.0
50	15,590 ± 90	—	4.0	6.5	9.0	11.5	11.5
75	15,550 ± 120	—	3.0	4.5	7.3	8.5	8.0
100	15,300 ± 240	—	1.5	2.0	1.0	3.0	1.0

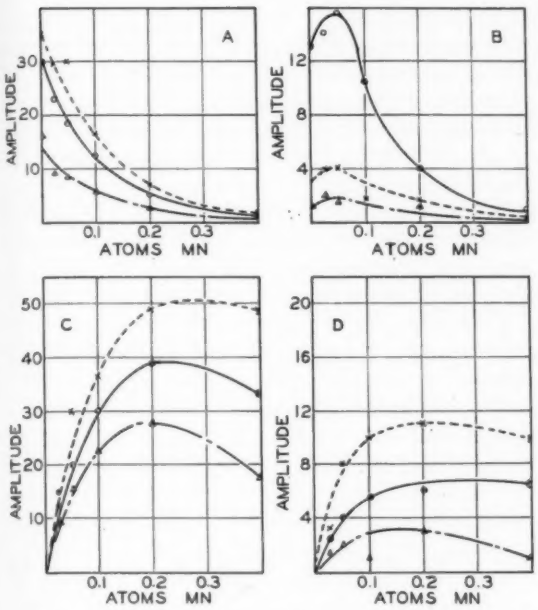

FIG. 3. Effect of manganese concentration on amplitude of Gaussian bands as affected by fluoride to chloride ratio used in the unfired mixture.

A—major antimony band —○——○— = 0% Cl
B—minor antimony band – ×– – – –× – = 30% Cl
C—major manganese band —△– – –△— = 100% Cl
D—minor manganese band

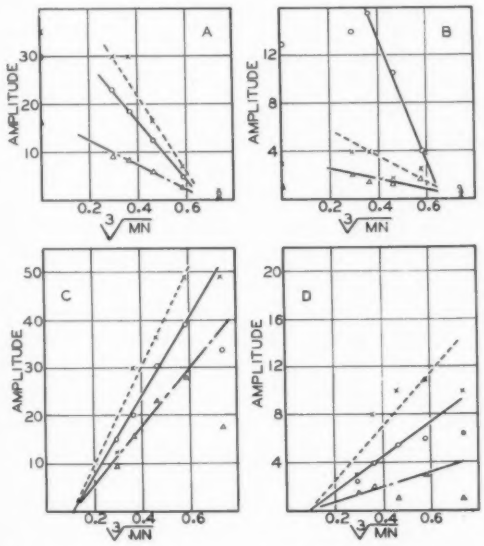

FIG. 4. Amplitude of Gaussian bands vs. cube root of manganese concentration.

A—major antimony band —○——○— = 0% Cl
B—minor antimony band – ×– – – –× – = 30% Cl
C—major manganese band —△– – –△— = 100% Cl
D—minor manganese band

falls off rather rapidly at first and then more slowly. Thus the overall effect of increasing chloride is to shift the emission color from the blue toward the blue-green.

The addition of manganese causes a rather sharp decrease in the amplitude of the major antimony band immediately, and a more gradual decrease in the minor band after the manganese concentration has built up to about 0.05 atom of manganese. Thus, the effect of manganese is to suppress gradually the antimony bands with the energy being transferred to the manganese bands in the yellow and orange regions of the spectrum. Fig. 3 shows on a linear scale the changing amplitude of the four components as affected by Mn content at three different chloride to fluoride ratios[2], while Fig. 4 gives part of the same data with the abscissa being the cube root of the manganese content, which approximates the linear concentration of manganese atoms along a given axis.

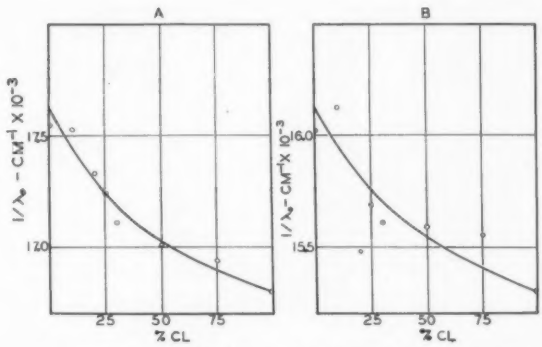

FIG. 5. Effect of chloride to fluoride ratio in the unfired mixture on position of manganese bands of the final phosphor. A—major band, B—minor band.

The invariance of position of the antimony bands simplifies the analysis of the spectrum, since they can be subtracted from the experimental curve leaving a residue for further analysis—this residue representing the emission of manganese alone.

It was found that the behavior of the manganese emission is considerably different from the emission in silicate phosphors. The emission is composed of a major and a minor band with the major band being approximately four times as intense as the minor. In addition to these two bands, certain of the spectral energy curves cannot be fitted by the use of two Gaussian curves but show a small residue in the deep red peaking beyond 6700 Å. We believe this is an indication of a third component and, in this respect, the system resembles zinc orthosilicate which showed one major and two minor components.

[2] The per cent chloride given refers to the raw material mixture. In the final phosphor the ratio of chloride to fluoride is somewhat lower for those cases where both halides are present, but this ratio is not affected appreciably by changing manganese contents.

With constant chloride to fluoride ratio, the intensity of both components increases to a maximum at about 0.20 atom of manganese and then drops off as the manganese content is further increased probably due to a quenching effect. The relative amplitude of the two manganese bands remains essentially constant over the whole range of composition studied. With constant manganese content but with variable chloride content, the location of both peaks shifts gradually toward longer wavelengths as the halide changes from 100 per cent fluoride to 100 per cent chloride. This shift amounts to about 250 Å, with the major band going from 5700 Å to 5950 Å and the minor band from 6250 Å to 6500 Å. Fig. 5 shows the gradual shift of the position resulting from changing chloride to fluoride ratio.

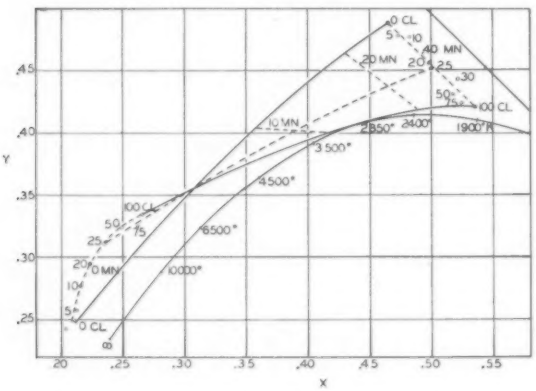

FIG. 6. Coordinates x, y, of fluorescent light from halophosphates on I.C.I. color mixture diagram.

I. C. I. Diagram for Halophosphates

The effect of variations in composition on the color of fluorescence of the halophosphates is shown in Fig. 6. This is a portion of the I.C.I. color mixture diagram and shows the points representing the colors of the various phosphors as they fluoresce in 20-watt lamps. These points were computed from the spectral energy distribution of the lamps, as measured by our spectroradiometer, using the Selected Ordinate method of integration. The points shown are for the color of the phosphor alone in order to eliminate the effect of brightness. In the normal fluorescent lamp the mercury arc contributes approximately a constant amount of light, assuming a constant optical density of powder on the bulb and good control of processing procedures. This light has color parameters in the neighborhood of $x = y = 0.218$. The effect of this contribution to the overall color of the lamp is to move the point on the I.C.I. color mixture diagram from that of the phosphor alone along the straight line joining that point and the mercury arc point with the amount of this shift being inversely proportional to the brightness of the phosphor. For example, with a phosphor of high intensity, the mercury arc contribution is relatively small and the color shift is slight, but when the phosphor has very low intensity, the contribution of the mercury arc to the total output is considerable and the color shift is large.

For clarity, only the curves for the extremes of chloride content and that of a median value are drawn on the chart with all data on the effect of varying chloride being shown on the lines for 0.0 and 0.4 atom of manganese. These curves show the wide variation in color which can be obtained with these phosphors.

The interesting facts shown by this chart are:

1. The curves for constant chloride content roughly parallel the locus of black body radiators and intersect each other at a point in the blue-green portion of the chart.

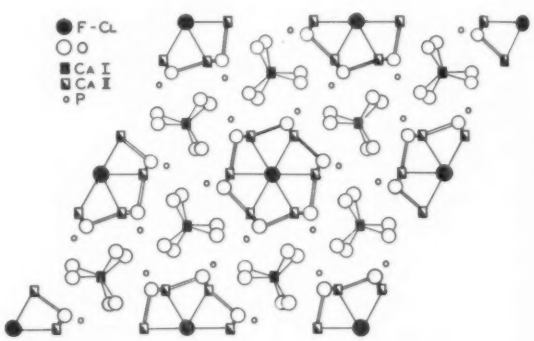

FIG. 7. Crystal structure of apatite

2. The lines of constant manganese are straight, with the exception of the zero manganese line, which shows a curvature toward the red with increasing chloride. The orientation of these lines shows a steady rotation through about 135° clockwise as the manganese in increased from zero to 0.40 atom.

3. A small amount of chlorine has a large effect on color. Thus the substitution of 25 per cent of the fluoride by chloride shifts the color more than half way toward that of 100 per cent chloride phosphor.

DISCUSSION

The calcium halophosphate phosphors are a particularly interesting addition to the growing number of double-activated phosphors, not only because both emission bands are in the visible spectrum, but also because of the complexity and unusual nature of the crystal structure. This crystal structure is well known since it is that of a common mineral, apatite, which has been thoroughly investigated by x-ray methods (8, 9, 10). Fig. 7 shows the projection of four unit cells on the 001 plane. It will be seen that the halide

ion is a key point in the structure, with two of these ions, arranged along the C axis, being present in each unit cell. The cell dimensions for fluo-apatite are $A_0 = 9.37$ Å, $B_0 = 9.37$ Å, and $C_0 = 6.88$ Å. Replacement of the fluoride by chloride results in an expansion along the A and B axis and a contraction along the C axis. A similar expansion and contraction of considerably smaller magnitude results from the substitution of manganese for calcium[3]. The position of halide ion depends on whether it is fluoride or chloride. The fluoride ions are placed $\frac{1}{4}$ and $\frac{3}{4}$ of C_0 above the base plane (001), while chloride ions are on the base plane and $\frac{1}{2}$ C_0 above it.

The calcium halophosphates are more readily adaptable to study by chemical methods than most phosphors since they are readily soluble in cold dilute acids. Our chemical investigations have established that manganese is present as a divalent ion and that the small amount of antimony present in acid soluble form is almost certainly trivalent. The remaining antimony is present as a separate phase which is insoluble in acids (11).

In the calcium halophosphate structure there are two types of calcium present—one of which is indicated as Ca I in Fig. 7. This type of calcium ion is completely surrounded by six oxygen atoms and is several atomic diameters distant from the halide ion, so that the strength of the calcium-oxygen bond would be very little affected by a substitution of chloride for fluoride. The invariant position of both of the components of the antimony emission band suggests that antimony enters the lattice as a replacement for Ca I with a group of two antimony ions and one additional oxygen ion replacing two calcium ions as indicated in Fig. 8. With antimony in this position the magnitude of the energy changes on excitation and emission should be very little affected by the composition of the phosphor[4].

The energy level diagram of trivalent antimony is quite simple with the base state being an even $^1S_0$ state and the excited odd levels being $^3P_0^\circ$, $^3P_1^\circ$, and $^3P_2^\circ$ in order. We may speculate that the antimony electrons are excited both to the "allowed" $^3P_1^\circ$ state and to either the $^3P_2^\circ$ or the $^3P_0^\circ$ "forbidden" state and that the probability of reaching a given state is influenced by surrounding ions, even if not near neighbors, so that replacement of fluoride by chloride or of calcium by manganese would change these probabilities, thus affecting the relative amplitude of the two components in the emission spectrum. The influence of such replacements is not sufficient, however, to affect the actual magnitude of the energy transitions, and, therefore, the components have an invariant frequency.

The second type of calcium ion present in the halophosphate structure is shown as Ca II in Fig. 7. These ions are directly bonded to the halide ions and their surroundings include both the halide and the oxygen ions. Due to the different position of fluoride and chloride in the lattice, the surroundings of these calcium atoms are considerably different in the two cases. It seems probable that manganese replaces Ca II and that the gradual shift of the band centers of the two components of the manganese emission can be explained by the changing proportions of manganese bonded to fluoride and manganese bonded to chloride. There is a difference in the number of calcium or manganese ions surrounding the halide ion due to the different location of the two types of ion on the C axis. The different strength of these bonds would shift the potential energy curves appreciably and the radiative transition from odd to even states would have appreciably different energy values, depending on whether the manganese was bonded to fluoride or chloride.

We may hypothesize that in calcium halophosphate the excited electron of the manganese ion

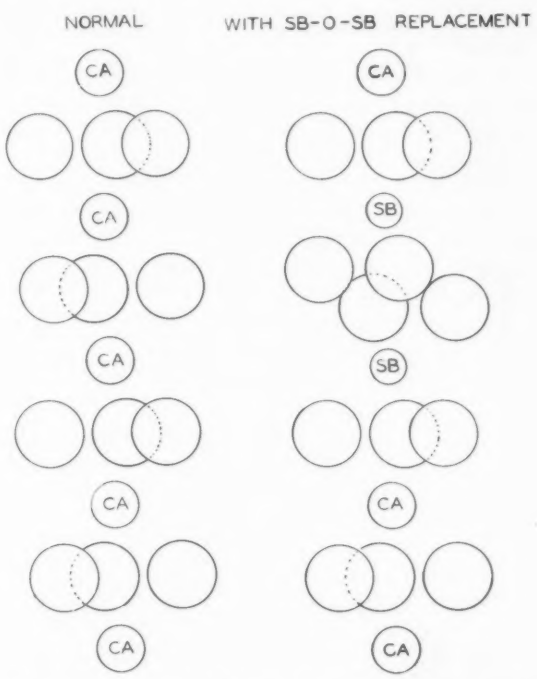

FIG. 8. Arrangement of atoms along Ca I axis in apatite

[3] This result is different from that found by Jenkins, McKeag, and Ranby, who report an expansion because of chloride and a contraction because of manganese.

[4] The probability of the transitions is affected by composition, especially by introduction of manganese, so that a high manganese phosphor shows only slight emission due to antimony. This change in transition probability for the primary activator, caused by the secondary activator, is characteristic of all double-activated phosphors.

always goes to the same odd level and that transitions from this to two different even levels account for the two components in the emission spectrum, while the tail in the spectrum at 6700 Å may represent excitation to a different odd level.

Conclusions

The behavior of the halophosphate phosphors conforms generally to theories previously proposed and we may restate some of the hypotheses of these theories (1, 12) in slightly different form:

1. Each component of the emission is due to a particular electronic transition. The position and shape of the band are determined by the energy levels of the activator ion, as affected by the influence of interatomic spacing on the potential energy curves.

2. The number of components and their position in the spectrum is considerably affected by the crystal lattice of the matrix and by the location of the activator ions in this matrix.

3. Increase in activator concentration does not affect the location of the emission band in the spectrum but does change the relative intensity due to changes in the probability that a particular energy transition will occur.

Differences between the behavior of the halophosphate phosphors and silicate phosphors, as interpreted here in terms of crystal structure, lead to two additional hypotheses:

4. The probability that a particular energy transition will take place is influenced not only by ions which are near neighbors of the activator but also by ions some distance away. The ions at a distance do not affect, however, the actual magnitude of the energy transition.

5. Change of the near neighbors to which the activator ions are directly bonded will cause a change in the location of the emission band by affecting the magnitude of the energy transition. This change in surroundings may also affect the probability of transitions.

Any discussion of this paper will appear in a Discussion Section to be published in the June 1951 issue of the Journal.

REFERENCES

1. K. H. Butler, *J. (and Trans.) Electrochem. Soc.*, **93,** 143 (1948).
2. G. Szigeti and E. Nagy, *Univ. for Tech. Sci., Budapest,* Publication #3 (1948).
2a. E. Nagy, *J. Optical Soc. Am.*, **39,** 42 (1949).
3. H. Brinkman and C. C. Vlam, *Physica,* **14,** 650 (1949); **15,** 609 (1949).
4. H. G. Jenkins, A. H. McKeag, and P. W. Ranby, *J. (and Trans.) Electrochem. Soc.*, **96,** 1 (1949).
5. R. Nagy, R. W. Wollentin, and C. K. Lui, *J. (and Trans.) Electrochem. Soc.*, **95,** 187 (1949).
6. S. L. Parsons, A. E. Martin, and S. N. Roberto, *J. (and Trans.) Electrochem. Soc.*, **97,** 41 (1950).
7. C. W. Jerome, *Illum. Eng.*, **45,** 225 (1950).
8. St. Naray Szabo, *Z. Krist.*, **97,** 387 (1930).
9. M. Mehmel, *Z. Krist.*, **75,** 323 (1930).
10. S. B. Hendrieks, M. E. Jefferson, and V. M. Mosley, *Z. Krist.*, **81,** 352 (1932).
11. K. H. Butler, V. M. B. Hannaford, and M. J. Bergin, *J. (and Trans.) Electrochem Soc.*, **97,** 117 (1950).
12. K. H. Butler, *J. (and Trans.) Electrochem. Soc.*, **95,** 267 (1949).

Studies on Galvanic Couples

I. Measurement of Electromotive Force and Internal Resistance of Cells during Current Flow[1]

H. D. Holler

National Bureau of Standards, Washington, D. C.

ABSTRACT

A method of measuring the effective electromotive force and internal resistance of a galvanic cell during current flow is described. A dry cell was used for demonstration of the method. By introducing a reference electrode into a cell consisting of an iron electrode and a magnetite electrode in wet clay, it was possible to measure the potential and resistance between the reference electrode and either the iron or magnetite during current flow. When the iron and magnetite were short-circuited, the potential and resistance between the reference electrode and the iron-magnetite couple were measured. By impressing current upon the galvanic couple from an auxiliary electrode, the potential-current characteristic of the couple was determined. It was shown that an iron plate in wet clay exhibits such a characteristic similar to that of the galvanic couple.

Introduction

In the measurement of internal resistance of a galvanic cell delivering current it is often assumed that the electromotive force maintains its open-circuit value. The emf driving the current is not necessarily constant, because a counter emf of polarization is usually generated, as the result of current flow. According to Ohm's law, the exact relationship is

$$\frac{E_1 - \Delta E_1}{R + r} = \frac{E_d}{R + r} = i \qquad (I)$$

where E_d = driving emf.
E_1 = open-circuit emf.
ΔE_1 = counter emf of polarization.
R = external resistance.
r = internal resistance.
i = current.

If E_d were measurable for known values of i and R, then r may be calculated from the above equation; or if r were known, E_d may be calculated. Also, since E_1 may be measured directly on open-circuit, the emf of polarization ΔE_1 may be found from the difference $E_1 - E_d$. Both ΔE_1 and E_d, and also the internal resistance, may vary considerably with the magnitude and direction of the current. These variations of E_d and r with current are, of course, manifestations of electrochemical processes occurring at the electrodes. We are dealing, therefore, with polarization phenomena and the problem is not only to measure the driving emf and internal resistance of a working cell, but also the potentials of the individual electrodes, and to indicate the role of the resistive components of the measured potential differences.

The measurement of electrode potentials without including the resistive components during current flow has long been a controversial problem (1). It is particularly important (*a*) when the reference electrode cannot be in intimate contact with the electrode under investigation, or (*b*) when the electrode is covered with a film of high resistance.

Moreover, since any electrode may exhibit potential differences on its surface, giving rise to currents flowing from anodic to cathodic areas, it is effectively a system of galvanic couples. Therefore, its behavior, in a cell through which current is flowing, should be in accordance with the electrical relations governing the polarization of galvanic couples. So far as the writer is aware, the measurement of emf and internal resistance of cells has not been approached from this viewpoint: that electrodes usually act like galvanic couples. Any departure from this role is one of degree only.

A Wheatstone bridge having an adjustable counter emf for measuring emf without including the resistive component has been used (2). This idea, together with modification of the bridge suggested in this paper, makes it possible to measure both the emf and internal resistance directly.

In addition, the technique described herein facilitates the use of a recording potentiometer for obtaining emf-time curves, provided the resistive component due to cell current does not change simultaneously.

Development of Technique

In developing this technique, it is necessary to consider the inherent properties of the Wheatstone

[1] Manuscript received September 29, 1949. This paper prepared for delivery before the Chicago Meeting, October 12 to 15, 1949.

bridge. For example, in Fig. 1 which represents the simplest bridge circuit, if the resistances have such values that

$$\frac{r}{x} = \frac{Q}{D} \qquad \text{(II)}$$

then closure of key K in the branch containing the emf b will cause *no deflection* of galvanometer g. This is the condition of a balanced bridge. A resistance R_K may be used in parallel with K to limit the change in voltage applied to the bridge, when the key is closed, and thereby control sensitivity.

Let us now replace r with a cell having an emf E_d and an internal resistance r, as in Fig. 2, where r has the same value as in Fig. 1. There is now a deflection of the galvanometer due to E_d. If the value of r changes, the bridge may be rebalanced with respect

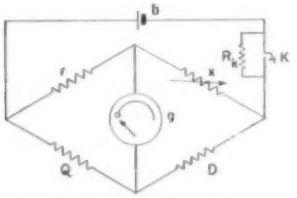

FIG. 1. Most elementary Wheatstone bridge

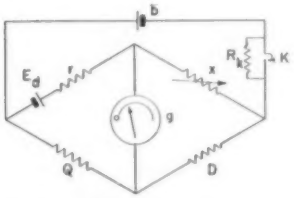

FIG. 2. Elementary Wheatstone bridge with emf in one arm.

to the resistive component by varying X until closing or opening K causes *no change* in deflection.

Let us now see how the value of E_d may be measured. If an adjustable counter emf V_g is put in series with the galvanometer, we have the relations shown in Fig. 3. Then according to Kirchoff's laws: in circuit (2):

$$E_d - V_g = ir + i_g r_g - (I - i)Q. \qquad \text{(III)}$$

r_g being the galvanometer resistance; in circuit (3)

$$V_g = (i - i_g)X - i_g r_g - (I - i + i_g)D. \qquad \text{(IV)}$$

Now, if $r = X$ and $Q = D$, then when i_g is reduced to zero by adjusting V_g until the galvanometer reads zero

$$E_d = 2V_g. \qquad \text{(V)}$$

This is true for any equal values of Q and D. Using the same circuits of Fig. 3, the relation between E_d and V_g may also be derived by the use of determinants.

As Pearson has shown (2), the adjustable counter emf may be used in the same arm of the bridge containing the emf to be measured, and the latter be read directly as V_g. However, the circuit described here more readily permits the galvanometer and adjustable counter emf to be replaced by a recording potentiometer for obtaining emf-time curves for the cell through which current is flowing. If r should vary with current, the bridge may be rebalanced by adjustment of X, giving r directly. This may be done as described above, or with alternating current.

Application of Technique

Dry Cells

The main objective in this work was the study of cathodic protection, but the adaptability of the cir-

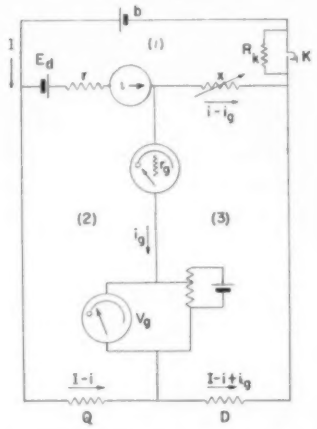

FIG. 3. Wheatstone Bridge with emf in one arm and an adjustable counter emf in series with galvanometer.

cuit in Fig. 3 to the measurement of emf and internal resistance was demonstrated by applying it to dry cells. Two aged cells of miniature size, having a high internal resistance, were used for the tests. The potential difference V across the cell during current flow was measured with a high-resistance potentiometer. Then

$$V = E_d \pm ir \qquad \text{(VI)}$$

in which all quantities depend on the magnitude and direction of i.

In order to compare the values of r, measured with alternating or direct current, 60-cycle current was also used for balancing the bridge, in which an a-c galvanometer served as null detector. The results of measurements are given in Tables I and II, and in Fig. 4. The resistances of Q and D were each 100,000 ohms. The galvanometer had a period of 1.4 seconds

TABLE I. *Internal resistance and driving emf of an aged dry cell for different currents*

Current i(ma)	Resistance r(ohms)	E_d (volts)	V volts	$(E_d - ir)$ volts
		Discharge		
1.00	470	1.220	0.740	0.750
0.83	470	1.220	0.838	0.830
0.60	420	1.226	0.991	0.974
0.25	250	1.244	1.112	1.084
		Charge		
				$(E_d + ir)$
0.33	163	1.264	1.353	1.340
0.69	123	1.346	1.429	1.431
0.98	105	1.396	1.500	1.499

TABLE II. *Comparison of results of measurement of internal resistance of an aged dry cell, using direct and alternating current for balancing bridge*

Current i(ma)		Internal Resistance r(ohms)	
		d-c	a-c
		Discharge	
1.10	Time effect*	350	350
1.10	Time effect	312	313
1.10	Time effect	300	306
0.90		299	300
0.60		280	282
0.35		203	197
		Charge	
0.15		140	132
0.30		119	117
0.50		120	116
0.73		116	116

*"Time effect" indicates drift in readings during measurement.

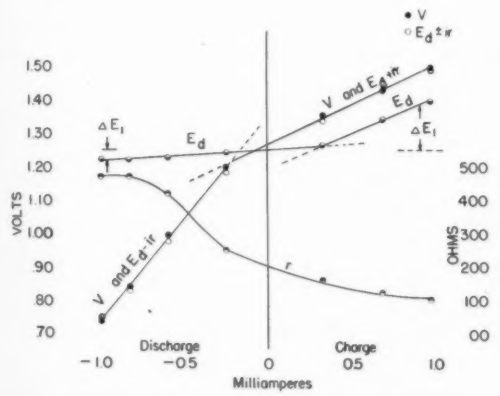

FIG. 4. Measured values of internal resistance and emf of dry cell during flow of current.

and a sensitivity of 0.0070 microamperes per division. A short period is necessary in order that any deflection, due to an unbalanced bridge, will occur quickly and before any slower deflection caused by cell polarization.

The agreement between the values of the potential difference V across the cell obtained by direct measurement, and the algebraic sum, $E_d \pm ir$, is very satisfactory at the higher currents, showing that the measured value of r truly represents the effective internal resistance. At the lower currents, agreement was not so good because of lower sensitivity. Even though r changes with time, as well as with current, the results with direct and alternating current are in satisfactory agreement. No doubt, the values of the bridge resistances could be so chosen that lower or higher values of internal resistance may be accurately measured.

The internal resistance of these two dry cells is directional, as indicated by the values lower on charge than on discharge. This might be explained on the basis of dry-cell theory and experimentally by the use of a half-cell for investigating the zinc electrode and the carbon-manganese dioxide electrode separately. This was not done, since other electrodes

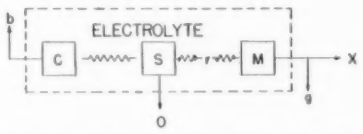

FIG. 5. Diagram showing introduction of half-cell S into cell under investigation.

were of primary interest, and we leave the subject of dry cells here.

Measurement of Electrode Potentials

Let us now consider modification of the circuit in Fig. 3 for measurement of a single electrode potential paired with a reference half-cell. For example, in Fig. 5 the cell consists of two electrodes, carbon C and a corrodible metal M such as iron, in an electrolyte, and between them is a reference half-cell S. Let r be that part of the internal resistance between S and the iron electrode, the latter being under investigation. Let this assembly in Fig. 5 be substituted for E_d and r in Fig. 3, and let E_x = the potential of the carbon electrode.

Then if the bridge is balanced by varying X until the closing or opening of key K causes *no change* in galvanometer deflection, and V_g is adjusted until the galvanometer reads zero, it follows that

$$r = X \qquad \text{(VII)}$$

and

$$E_M - E_s = 2V_g \qquad \text{(VIII)}$$

where E_M = the potential of the metal electrode, and E_s = the potential of the reference half-cell.

The reference half-cell used here was the carbon-manganese dioxide electrode of a dry cell. This electrode was made up by substituting, for the zinc can, a Lucite tube having a porous diaphragm which permitted electrolytic contact with the cell under investigation. It was designed for ruggedness in field work, and was used here because of convenience.

The values of the fixed equal arms of the bridge may be increased if necessary to reduce the current through the half-cell, and therefore its polarization, or they may be decreased to improve the sensitivity of the bridge.

In the measurement of electrode potentials in various electrolytes, it is soon realized that a metal does

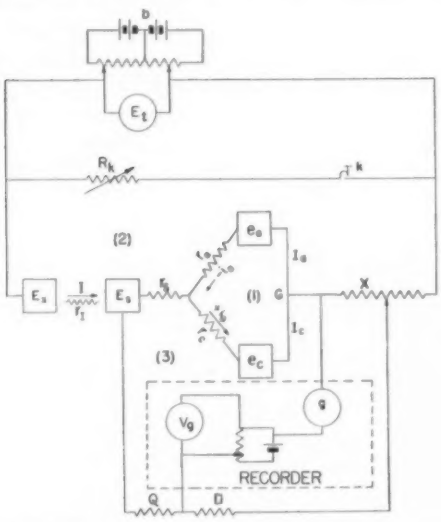

FIG. 6. Diagram showing technique of measurement of emf and resistance for different values of E_t and I; also possible resistances in couple and introduction of potentiometer recorder.

not usually exhibit its own potential, but behaves like a galvanic couple; that is, its observed potential lies somewhere between the potentials of the anodic and the cathodic areas on the surface.

If in Fig. 6 we let e_a and e_c be the polarized potentials of the anodic and cathodic areas, respectively, and r_a and r_c be the corresponding resistances of the current paths between the half-cell and the same areas, ignoring r_s for the moment, then the potential of the metal electrode, with reference to the half-cell S, may be represented by equation

$$E_G = e_a - i_o r_a \qquad \text{(IX)}$$

$$= e_c + i_o r_c. \qquad \text{(X)}$$

Since $E_G = 2V_g$, a potentiometer recorder may be introduced in Fig. 6 and calibrated to record E_G directly. A resistance R_K may be used in series with K to vary sensitivity as in Fig. 6, or in parallel with K (Fig. 3).

Resistance of a Galvanic Couple

In the Wheatstone bridge circuit, the metal electrode, behaving like a galvanic couple, will exhibit a certain resistance R_G toward the bridge (external) current I. If E is the potential difference applied to the couple which is equal to $E_t - E_x - I(r_1 + r_s)$, then from Ohm's law

$$\frac{E - E_G}{I} = R_G. \qquad \text{(XI)}$$

To evaluate R_G, consider the circuit in Fig. 6 where

$$\frac{E - e_a}{r_a} = I_a \qquad \text{(XII)}$$

and

$$\frac{E - e_c}{r_c} = I_c. \qquad \text{(XIII)}$$

Neglecting the small current through Q and D, $I_a + I_c = I$. Adding we have

$$\frac{r_c(E - e_a) + r_a(E - e_c)}{r_a r_c} = I. \qquad \text{(XIV)}$$

But

$$e_a - e_c = i_o(r_a + r_c) \qquad \text{(XV)}$$

which is independent of I.

At this point, it must be emphatically realized that the local current i_o is determined entirely by $e_a - e_c$ for given resistances in the network. Any effect which the external current I may have on i_o is the result of electrochemical action on $e_a - e_c$. Electrically, I and i_o are independent of each other.

Substituting the value of e_c from the preceding equation, in equation (XIV), and simplifying, gives

$$\frac{(r_a + r_c)(E + i_o r_a - e_a)}{r_a r_c} = I. \qquad \text{(XVI)}$$

Then introducing the value of $E_G = e_a - i_o r_a$ from equation (IX) we have

$$\frac{E - E_G}{I} = \frac{r_a r_c}{r_a + r_c}. \qquad \text{(XVII)}$$

Therefore, from equations (XI) and (XVII)

$$R_G = \frac{r_a r_c}{r_a + r_c}. \qquad \text{(XVIII)}$$

This equation may also be derived from the same circuits by the method of determinants, for any value of I, regardless of the magnitude or direction of I or i_o.

If, therefore, the bridge be balanced and the galvanometer reading be brought to zero by adjustment of V_g then

$$E_G - E_s = 2V_g \qquad \text{(XIX)}$$

and

$$X = r_s + R_G \qquad \text{(XX)}$$

where r_s is a series resistance depending on the location of the half-cell and the configuration of the electrode under investigation.

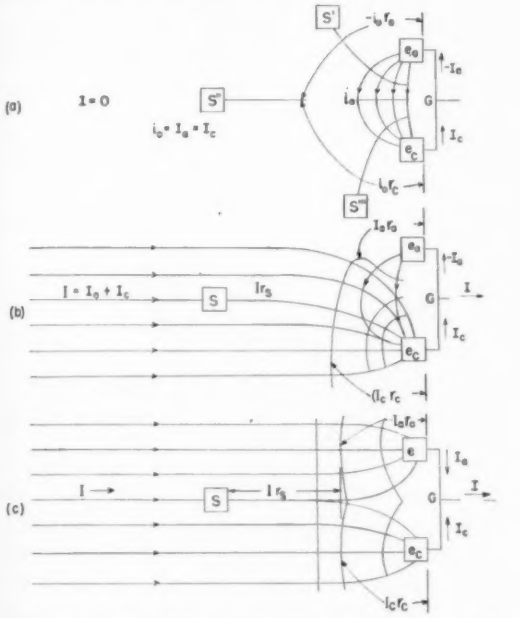

FIG. 7. Diagrams showing relation of position of half-cell S to couple and effect of I and series resistance r_s on observed values of E_g.

Relation of Position of Half-Cell to Observed Potential of Couple

These relations may be more easily visualized if we consider currents I and i_o superimposed on each other, their directions being determined by the emfs causing them; the resistance of the couple behaving like the resistances of the two paths in parallel.

When $I = 0$, the observed value of $E_G - E_s$ depends on the position of S, as shown in Fig. 7(*a*), where the equipotential levels S', S'', and S''' are indicated. Any change in the position of S along one of these levels should not affect its potential reading. If the potential levels be unknown, then tests at various distances, say at S'' on a line perpendicular to the surface of the electrode, may be made in order to find an area in which further changes in position of the reference electrode make negligible differences in the readings. This may be considered a "remote" position.

If an external current I is impressed from a distant source, we have the situation in Fig. 7(*b*), where the potential levels have been distorted by introduction of the resistive component Ir_s. The total resistive component of the potential difference between S and G is $Ir_s + I_c \cdot r_c$ along the cathodic path, or $Ir_s + I_a r_a$ along the anodic path, where r_s is common to both paths. The potential of the couple, referred to S, *including all resistive components* is then

$$E_G + I(r_s + R_G). \qquad \text{(XXI)}$$

This is the value which would be obtained if the potential difference were measured with a potentiometer.

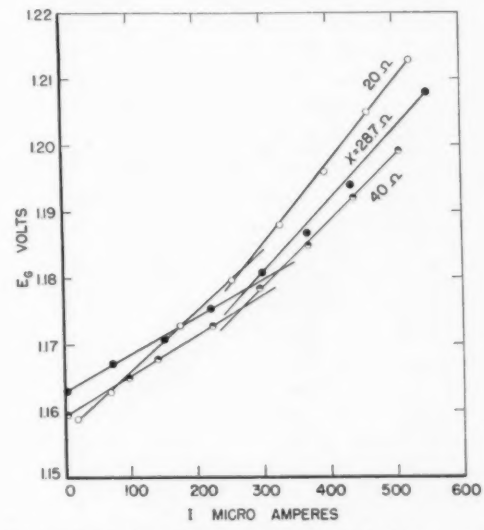

FIG. 8. Data showing characteristic E_g/I of iron cathode for different settings of bridge.

Now, if I is increased until the potentials of the cathode and anode become equal, then I_a becomes zero. On further increase of I, I_a becomes positive, flowing to the electrode, formerly the anode. Then r_s may be defined as that resistance, through which all of I flows, extending from S to a point where the current divides between the anodic and cathodic paths. The resistance from this point on to G via anode path is r_a, and via cathode path r_c, the total resistive component between S and G as measured by a Wheatstone bridge being

$$I(r_s + R_G). \qquad \text{(XXII)}$$

Using the technique of first balancing the bridge and then adjusting the counter emf V_g until the galvanometer reads zero (Fig. 6), we actually subtract the resistive component, represented by (XXII), from (XXI) and obtain E_G.

Technique Applied to an Iron Electrode

The resistances, r_a and r_c, are in series in the closed galvanic couple circuit (1), Fig. 6, but they are in parallel with reference to I which is also the bridge current. They may vary as a result of the passage of current in such a way that R_G may be changed. However, it is also possible for the enlargement of the current path to the cathode to occur, at the expense of the anode path, without changing R_G, unless the resistance of the anode path depends on direction of current.

By applying the above technique to an iron-plate electrode, 2 in. x 6 in. (5.1 x 15.2 cm), immersed in wet clay in a small container using a carbon-manganese dioxide electrode for reference, the graphs in Fig. 8 were obtained, where $X = 28.7$ ohms.

A discontinuity in the graph for $X = 28.7$ ohms occurred at potential $E_G - E_s$ of about 1.178 volts, which was not far from the open-circuit potential of iron for the conditions given. A current of about 275 microamperes was required to make the iron plate behave as if it were cathodic, although the current density on its back surface must have been low. In a larger container, the current density would be more uniform and the possibility of any anodic areas on the back surface would be less. Then, the potential, at which the discontinuity occurs, should be nearer to the open-circuit potential of iron.

Changing the bridge setting from 28.7 to 20 or 40 ohms is similar to changing the calibration of a meter, and resulted in different slopes, but the discontinuities all occurred at nearly the same current of 275 microamperes. Accurate balancing of the bridge, therefore, is not necessary to obtain a potential-current characteristic of the electrode. The similarity between this characteristic for the iron-plate electrode in Fig. 8, and that for the dry cell, suggests that the polarization characteristics of both are similar. The discontinuities in the values of E_d and V (Fig. 4) may be related to the polarization characteristic of one or both of the dry cell electrodes. On charge, the graph E_d may manifest a change in potential of the zinc cathode, similar to that for the iron in Fig. 8.

Apparent Film or Phase Boundary Resistance

In defining r_a and r_c as the resistance of the anodic and cathodic paths, respectively, it was tacitly assumed that the current distribution of I over the anode and cathode area was the same as that of i_o. This is not strictly true. Perhaps the best we can do in describing r_a and r_c is as represented in Fig. 6, where the two resistances are joined to a series resistance r_s. The order of magnitude of r_a and r_c may be determined for couples of specific electrodes, which may be measured separately or together.

For example, in the case of a couple consisting of a rod of iron and a similar rod covered with magnetite, both in wet clay, the following bridge measurements were made:

$$X_1 = r_s + r_a = 22.0$$
$$X_2 = r_s + r_c = 37.4$$
$$X_3 = r_s + R_G = 20.4$$

Then, since

$$R_G = \frac{r_a r_c}{r_a + r_c}$$

by using the quadratic formulae, the following values were obtained: $r_s = 16$, $r_a = 6$, and $r_c = 21.4$.

Thus it is apparent that r_c, or the apparent boundary resistance of the cathode, is $3\frac{1}{2}$ times greater than that of the anode. This is important in determining the partition of the current I between the anodic and cathodic areas. Thus

$$I_a = \frac{E - e_a}{r_a} \quad \text{and} \quad I_c = \frac{E - e_c}{r_c}. \qquad \text{(XXIII)}$$

Then

$$\frac{I_a}{I_c} = \frac{r_c(E - e_a)}{r_a(E - e_c)} \qquad \text{(XXIV)}$$

which shows that the partition of current I is determined by the opposing emf, as well as by the resistance of each path.

Conclusions

The driving emf of a cell and its internal resistance may be determined simultaneously by a bridge-potentiometer technique. Both of these vary with the magnitude and direction of current through the cell. Applying the theory of polarization of galvanic couples, the reasons for some of these variations are explainable. To a potentiometer alone, an emf and a resistive component of a potential difference look alike. Using a potentioneter and a bridge as described herein, it is possible to differentiate between these components to an extent, depending upon the galvanic couples involved. By the introduction of a half-cell, both the emf and resistive component of polarization of the individual electrodes may be determined, remembering that each electrode itself may behave like a short-circuited galvanic couple. The circuit developed herein may be used for recording the emf of a cell carrying current without inclusion of the resistive component.

Any discussion of this paper will appear in a Discussion Section, to be published in the June 1951 issue of the Journal.

References

1. H. D. Holler, *Bur. Standards Sci. Paper*, **20,** 153 (1924-26).
A. L. Ferguson, *Trans. Electrochem. Soc.*, **76,** 113 (1939).
E. Newbery, *Trans. Faraday Soc.*, **43,** 127 (1947).
2. J. M. Pearson, *Trans. Electrochem. Soc.*, **81,** 485 (1942).

Studies on Galvanic Couples

II. Some Potential-Current Relations in Galvanic Corrosion[1]

H. D. Holler

National Bureau of Standards, Washington, D. C.

ABSTRACT

A graphic method of expressing the electrical characteristics of a galvanic couple was developed by the application of Kirchoff's laws to a couple consisting of separate electrodes, each with an ammeter in series. When an external emf was impressed between the couple and a third electrode, also with an ammeter in series, a definite current pattern was established, depending on the relative directions and magnitudes of the impressed emf and the potential of the couple. These relations were demonstrated with the iron-magnetite couple. Under the conditions used, a discontinuity in the potential-current relation was observed, when the couple was cathodically polarized over a sufficient range of current. This discontinuity or "break" coincided with reduction of current, circulating within the couple, to zero. The rise in potential at this point is the logical result to be expected from the hydrogen overvoltage.

Introduction

In the measurement of the so-called "static" electrode potential of a metal in a given electrolyte, without measurable current flowing to or from the electrode, it is usually assumed that the measured value represents the potential of the metal itself. This can be true only when there is no local galvanic-cell activity on its surface. For example, if we put iron, the metal which concerns us most in this discussion, in air-free water, the following reaction occurs:

$$Fe(s) + 2H_2O(l) \rightleftarrows Fe(OH)_2(s) + H_2(g) \qquad (I)$$

which proceeds until a pH of about 9.5 is reached. This is determined by the solubility-product and stability of ferrous hydroxide.

We then have the galvanic cell

$$Fe/[Fe^{++}]/\ /[H^+]/H \qquad (II)$$

where the anodic reaction is,

$$Fe(s) \rightarrow Fe^{++} + 2\varepsilon \qquad (III)$$

and the cathodic process is

$$2H^+ + 2\varepsilon \rightarrow 2H \rightarrow H_2(g). \qquad (IV)$$

If we now introduce a third electrode such as the normal calomel, for reference, into the electrolyte and measure the difference in potential between it and the piece of iron, we obtain a reading which does not represent iron alone, but lies somewhere between the potentials of the iron anode and the hydrogen cathode. Thus in Fig. 1, the measured difference in potential is $E_G - E_s$ where E_G is the potential of the Fe/H couple, and E_s is that of the reference electrode, i_o being the cell current. Here, E_{Fe} = potential of iron, and E_H = potential of hydrogen, when $i_o = 0$.

The potential level E_G is determined by the emf components of polarization, ΔE_{Fe} and ΔE_H, and by the resistive components $i_o r_a$ and $i_o r_c$, where r_a and r_c are the resistances of the current paths between the reference electrode and the anode and cathode, respectively. All of these components are functions of i_o. If $i_o = 0$, then and then only, $E_G = E_{Fe}$, the true potential of iron.

Since E_H and, to a lesser extent, E_{Fe} depend upon the hydrogen ion activity of the electrolyte, the emf of the Fe/H couple is related to pH (Fig. 2) (1). The electrode potentials of hydrogen and iron become nearly equal at a pH value of about 9.5 and, consequently, the emf of the cell (II) approaches zero. Over a range of several pH units near the neutral point, e.g., from pH 5 to pH 10, E_{Fe} varies only a few millivolts, while E_H changes 58 mv per pH unit. At a pH 5, the emf of the Fe/H couple is about 0.20 volt.

While the approach of E_G toward the higher level of E_{Fe} caused by increasing values of ΔE_H will be accompanied by a reduction in i_o (cathodic control) and, therefore, in corrosion rate, it is possible under certain conditions that the polarization component ΔE_{Fe} may become very large with the result that E_G approaches the lower level of E_H, also accompanied by a reduction in i_o (anodic control), and consequently, a decrease in rate of corrosion by galvanic-cell action. It is apparent therefore, that the value of E_G alone should not be taken as a guide to indicate corrosion rate, and that an increase or decrease in E_G should not necessarily indicate an increase or decrease in corrosion rate; but its interpretation must be related to other simultaneous observations

[1] Manuscript received September 29, 1949. This paper prepared for delivery before the Chicago Meeting, October 12 to 15, 1949.

such as those obtained when the galvanic cell is subjected to applied external current.

Behavior of a Galvanic Couple toward External Current

The behavior of a galvanic cell toward an externally applied potential depends primarily upon the relative values, directions, and changes in emfs involved. If, for example, in Fig. 3, we impress a potential E_t between an iron-magnetite couple and an external electrode of carbon C, we obtain one of the Kirchoff patterns indicated. At this point, it should be pointed out that, since the activity of the couple results in liberation of hydrogen on the magnetite cathode, we are really dealing with the Fe/H cell represented in Fig. 1.

The potential E_x of carbon is below E_G and calomel in Fig. 1. Therefore, when an applied potential is gradually increased, beginning at zero, external current I will not flow to the couple until

$$E_t > E_G - E_x$$

and then it will flow first to the cathode because its potential is exceeded first. As E_t is increased, current will continue flowing to the cathode, until its potential becomes equal to E_{Fe}. Then, and then only, will current flow to the iron. This phenomenon depends entirely on polarization of the cathode, the term polarization being used in its broader sense to include both counter emf and the resistive component, caused by current flowing through resistance. When the applied potential E_t just balances the potential of the galvanic couple E_G, there is no external current. Then

$$E_t = E_G - E_x$$

$$I = 0$$

$$I_a = I_c = i_o \text{ (pattern } d\text{)}.$$

When there is no applied potential, current flows from the iron anode into the external circuit. Then

$$E_t = 0$$

$$-I = -I_a + I_c \text{ (pattern } c\text{)}.$$

When $E_t > E_G - E_x$, external current flows to the cathode (pattern e). Now, if the polarization of the cathode ΔE_H is increased, its potential moves toward that of iron. When

$$E_H + \Delta E_H + I_c r_c = E_{Fe} \text{ (Fig. 1)}$$

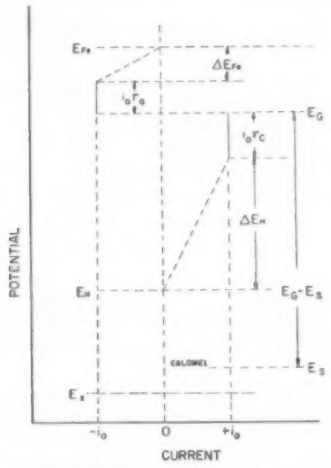

Fig. 1. Diagram showing electromotive force, $E_G - E_x$, between E_G, potential of iron-hydrogen couple, and E_x, potential of reference calomel electrode.

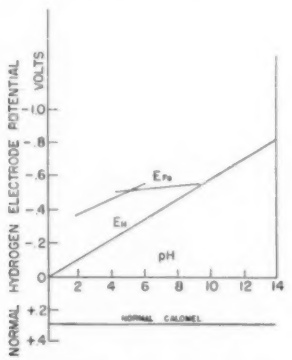

Fig. 2. Relation of potential, E_{Fe}, of iron in air-free electrolyte, (according to data summarized by Gatty and Spooner) to potential, E_H, of hydrogen at different pH values.

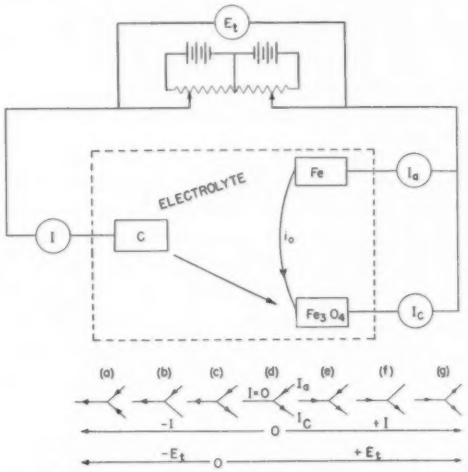

Fig. 3. Diagram showing technique for determining relation between applied potential, E_t, and currents through Fe/Fe_3O_4 couple and external electrode, carbon.

then

$$E_t = E_{Fe} - E_x$$

$$I_a = 0$$

$$I = I_c \text{ (pattern } f\text{)}.$$

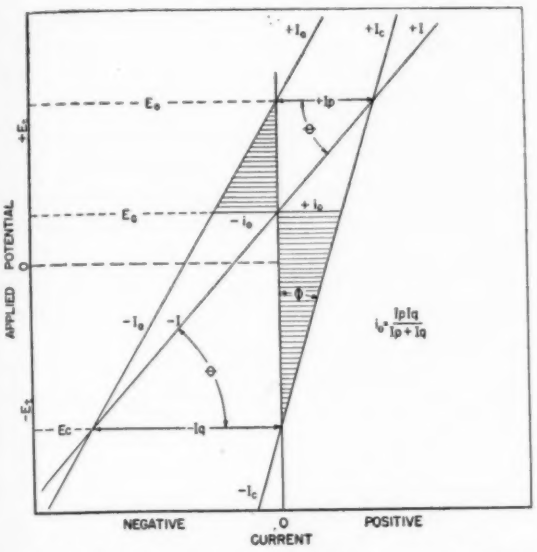

FIG. 4. Diagram showing hypothetical relations between applied potential, E_t, and I, I_a, and I_c.

On further increasing E_t above E_{Fe}, current flows to both electrodes. Then

$$E_t > E_{Fe} - E_x$$

$$I = I_a + I_c \text{ (pattern } g\text{)}.$$

Likewise, if the anode can be polarized by increasing E_t in the negative direction until

$$-E_t = E_H - E_x$$

then

$$I_c = 0$$

$$I = I_a \text{ (pattern } b\text{)}.$$

On further increasing E_t in the negative direction until

$$-E_t > E_H - E_x$$

$$-I = -I_a - I_c \text{ (pattern } a\text{)}.$$

If I, I_a, and I_c are plotted for different values of E_t, the relations shown in Fig. 4 are obtained. These graphs are not necessarily straight lines, but at the potential levels where

$$E_t = E_{Fe} - E_x$$
$$E_t = E_G - E_x$$
$$E_t = E_H - E_x$$

the current relations are rigidly fixed by Kirchoff's law. The galvanic-cell current i_o is indicated for the condition when $E_t = E_G - E_x$, that is, when $I = 0$. I_a is reduced to zero, when $E_t = E_{Fe} - E_x$. The value of I at this potential level is I_p, the "protective current," where the iron becomes wholly cathodic and is completely protected from corrosion. I_c may also be reduced to zero when $E_t = E_H - E_x$. The value of I at this level is I_q, but is not wholly protective since the couple is now all anodic, and may corrode in accordance with Faraday's law, or become passive.

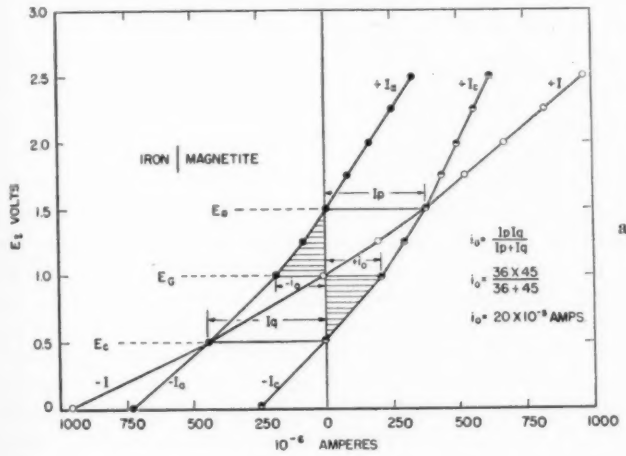

FIG. 5. Experimentally determined relations between applied potential E_t and currents I, I_a, and I_c.

By simple trigonometry

$$i_o = \frac{I_p I_q}{I_p + I_q} \quad (1)$$

When it is possible to estimate I_p and I_q, i_o may be calculated, even though not directly measurable.

In Fig. 5, actual readings on an iron-magnetite

couple are shown. The computed maximum value of i_o agrees very closely with the measured value, when $I = 0$. It is apparent that the graphs are not single straight lines, but generally intersecting straight lines. For example, at the current I_p, where iron becomes cathodic, there is evidence of a discontinuity. If we knew the slope of I_c, we could estimate the value of i_o. For example, in Fig. 5, the ratio $\alpha = i_o/I_p$ is approximately 0.6. An experimental determination of I_p, therefore, would show how much current is necessary to protect the anode from corrosion, and also, when multiplied by α would indicate the rate of corrosion without cathodic protection. The study of a number of such couples would tell us whether this ratio is characteristic of the couple. If it is, then the rate of corrosion is

$$\frac{W}{t} = \alpha I_p \cdot k \qquad (2)$$

at the value of I_p required to reduce I_a to zero. A similar pair of intersecting straight lines was obtained for an iron plate, which behaved like the galvanic couples under the same conditions. Inspection of the plate afterward indicated that the lower end was more seriously corroded than the upper area, presumably due to differential aeration.

If we consider the whole cell as represented in Fig. 3, then

$$E_t = E_G + I(R + r) - E_x \qquad (3)$$

where R = external resistance, r = internal resistance, and E_x = the potential of the carbon electrode. If the ratio E_x/I is a straight line relation, and $(R + r)$ is constant, any change in E_G will be reflected in the composite value, E_t.

In Fig. 7, the change in $E_G(\Delta E_G)$ produced by the polarizing current is also given for the iron plate in

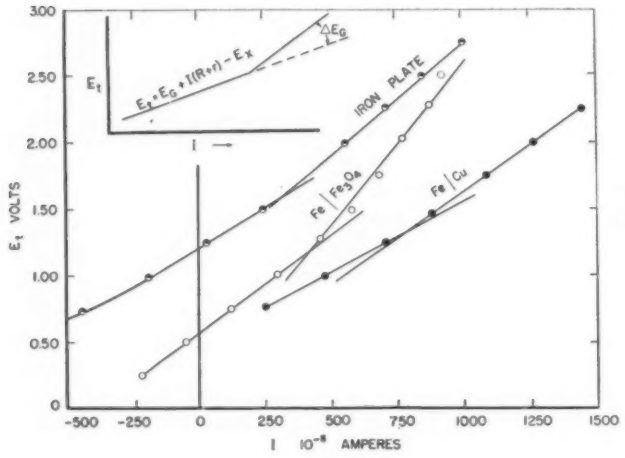

FIG. 6. Experimental relations between applied voltage E_t and external current, I, for Fe/Cu and Fe/Fe_3O_4 couples and for iron plate.

where W = metal lost by corrosion, t = time, and k = the electrochemical equivalent of the metal.

While it is clear that corrosion is stopped by the application of current I_p, experimental evidence of this fact is required. If E_{Fe} be known, then I_p is simply that current necessary to polarize the cathode until its potential $e_c + I_c \cdot r_c$ becomes equal to E_{Fe}. The requirement of this procedure is two-fold: first, a determination of E_{Fe} in the particular environment by a suitable technique, and second, a method of determining when the potential corresponding to $e_c + I_c r_c$ is attained.

Estimation of Protective Current

We have in Fig. 6, the relation between E_t and I for Fe/Cu and Fe/Fe_3O_4 couples in wet clay, which is representative of air-deficient conditions, where liberation of hydrogen may be expected. The intersection of the two straight lines in each case occurred wet clay. In this case, the reference electrode was a carbon-manganese dioxide electrode. The second derivative, obtained by plotting increments of ΔE_G for each increment of 250 microamperes, emphasizes the "break" which coincides with the intersection of the graphs, representing the relation between E_t and I.

Under extremely aerated conditions, no "break" was obtained. It would appear, therefore, that incipient liberation of hydrogen is necessary to account for the accelerated rate of increase of E_G, when the iron becomes cathodic, and is favored by practically air-free conditions Let us see why such an increase in the counter emf of polarization might be expected at this point.

When the galvanic couple becomes completely polarized cathodically, it behaves like a hydrogen electrode. Unlike metals, the potential of hydrogen depends not only upon the hydrogen ion concentration $[H^+]$, but also upon the pressure P of atomic

hydrogen at the surface of the metal. In accordance with Nernst's law, any increment in potential is given by the equation

$$\Delta E_g = \frac{0.058}{n} \log_{10} \frac{\Delta P}{[H^+]} \quad (4)$$

If $[H^+]$ is practically constant, then ΔE_g is a logarithmic function of ΔP. By Faraday's law, the rate of production of atomic hydrogen, and, therefore, also the rate of increase of P, is a linear function of current, at least initially. Consequently, ΔE_g is a logarithmic function of current, which is a characteristic of hydrogen overvoltage (1). Any decrease in $[H^+]$, due to alkalinity at the cathode surface, would result in a further increase of E_g. A depolarizer, such as air, tending to reduce the value of P, would result in a lower value of E_g.

In addition to an expected increase in counter emf due to hydrogen, a possible increase in electrical resistance due to a hydrogen film should not be overlooked. Some evidence of this resistive component in the increase in cathodic potential is available.

The value of I_p may, therefore, be considered as equivalent to the polarizing current required to increase E_g to the level where its relation to the current is that characteristic of hydrogen overvoltage. It may be determined from the relation of the applied voltage E_t, or of the galvanic potential E_g to the polarizing current I; or by polarizing E_g to E_{Fe} provided the latter is known in the given environment.

Up to the present moment, reference has been made only to current, whereas it is current density, multiplied by time, that really controls the electrochemical processes which cause polarization. Below I_p, all external current flows to the cathode, and in the case of the iron plate, the area of the cathode was unknown. Above I_p, the external current is distributed over the surface, now entirely cathodic, not necessarily uniformly, but in accordance with the resistance and counter emf of polarization. For example, let the polarized potential, $E_c + \Delta E_c$, of the area originally cathodic be e_c and, similarly, let the polarized potential, $E_a + \Delta E_a$, of the area originally anodic, be e_a. Then using increments, and Ohm's law

$$\frac{\Delta I_a}{\Delta I_c} = \frac{r_c(\Delta E - \Delta e_a)}{r_a(\Delta E - \Delta e_c)} \quad (5)$$

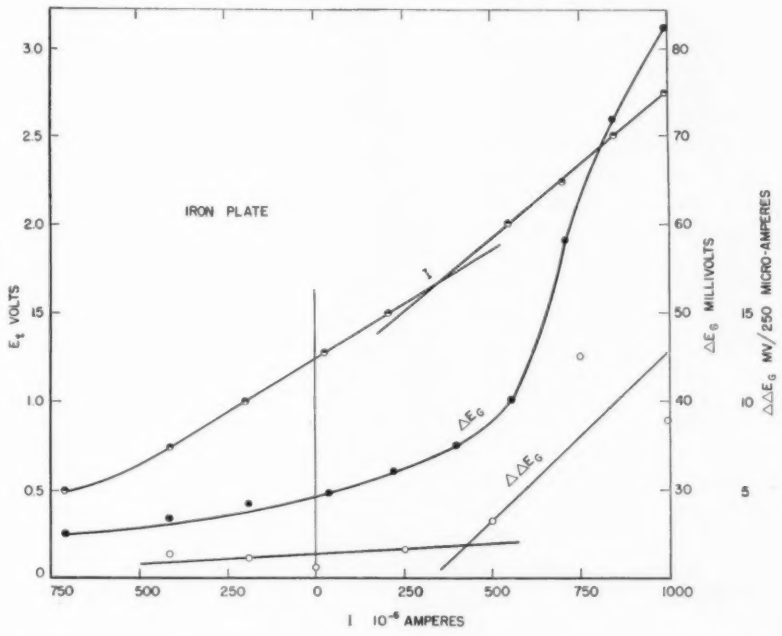

FIG. 7. Correlation of observed change in potential, ΔE_g, of iron cathode with E_t/I graph.

where ΔE is the increment in potential applied across the couple, and r_a and r_c are the resistances of the anodic and cathodic paths, respectively. Since ΔE_a and ΔE_c are functions of ΔI_a and ΔI_c, respectively, the current density tends to be more uniform than if governed by resistance alone (3). This is a fortunate circumstance in the application of cathodic protection.

CONCLUSIONS

The measurement of E_g by any suitable method and its relation to the polarizing current may serve to indicate the magnitude of the protective current. Under certain conditions, for example, in an air-deficient environment, this indication may be sharp. If conditions are not favorable to observance of the

usual overvoltage relation to current, estimation of the protective current from polarization curves may not be practicable. Fortunately, in underground corrosion, the air-deficient environment favors the interpretation of the results of this type of measurement.

If the above relations, established in the laboratory, can be determined in the case of pipe-lines and other underground structures, it may be possible to evaluate the total galvanic current flowing in the phase boundary and, therefore, the rate of corrosion at the moment; as a corollary, it may be possible to estimate how much externally applied potential or current is required to stop corrosion. It is believed that this may be possible, in many environments, for the simpler geometrical structures where distribution of current can be accomplished.

Any discussion of this paper will appear in a Discussion Section, to be published in the June 1951 issue of the the JOURNAL.

REFERENCES

1. O. GATTY AND E. C. R. SPOONER, "Electrode Potentials of Corroding Metals in Aqueous Solutions," Oxford Press, London, (1938).
2. A. THIEL AND J. ECKELL, *Z. Elektrochem.*, **33**, 370 (1927).
3. T. P. HOAR AND J. N. AGAR, *Far. Soc. Disc.*, **1**, 162, (1947).

Corrosion Rate and Etch Structures of Aluminum; Effect of Heat Treatment and Impurities[1]

B. Roald[2] and M. A. Streicher[3]

Lehigh University, Bethlehem, Pennsylvania

ABSTRACT

The effect of heat treatment of aluminum alloys ranging in purity from 99.2 to 99.998 per cent Al on the rates of dissolution and resulting etch structures in hydrochloric acid and sodium hydroxide solutions has been studied. The results are listed at the end of the paper under Summary.

Introduction

The present paper is a report of a brief morphological study of the effects of heat treatment and of impurities in aluminum on the rates of dissolution in hydrochloric acid and in sodium hydroxide solutions and the resulting etch structures. Although the electrochemical character of the dissolution process in both of these solutions appears to be well established, there are a number of apparently contradictory observations and interpretations in the literature on the effect of heat treatment of aluminum on its behavior in these solutions (2, 4, 9, 18).

Experimental

Two heat treatments were chosen, (*a*) all specimens were heated to 360° C to anneal the two phase structure present in all but the highest purity metal, and (*b*) some specimens were then heated at 575° C for 48 hours to produce a single phase structure in the purer specimens. One half of the latter specimens were furnace cooled and one half were water quenched from 575° C to determine the effect of cooling rate.

The compositions of the various types of aluminum used are given in Table I.[4] The specimens were punched in one piece from sheets 1–2 mm thick in the form of disks two inches (5.1 cm) in diameter with a 1½ inch (3.8 cm) handle. The handle was covered with a plastic coating leaving an exposed area of 40.5 cm². All specimens were heated to 360°C in an electric furnace and allowed to cool in the furnace. Some of these specimens were then, reheated in a Hayes furnace at 575°C for 48 hours, in two lots containing equal numbers of specimens of each aluminum alloy. One lot was water quenched from 575° C and the remaining lot was allowed to cool to room temperature in the furnace. The oxide coating formed during heat treatment was removed in 1*N* sodium hydroxide solution. Those specimens whose rates of dissolution in hydrochloric acid were to be determined were given a preliminary etch in hydrochloric acid to remove the sodium hydroxide etch structure formed during the removal of the heat treating scale.

Dissolution runs were made in one liter of 20 per cent hydrochloric acid at 25°C and in 0.30*N* sodium hydroxide in 4 liters of solution at 23°C. To obtain comparable and reproducible dissolution rates the initial surface of the aluminum must be uniform in its break-down characteristics throughout all tests. Therefore, the specimens were immersed in concentrated sodium hydroxide solution (6*N*) until hydrogen bubbles appeared (10–20 seconds) and were then rapidly withdrawn, rinsed immediately with water, and immersed in the test solution for a run.

Results

Thermal Treatments

The heat treatment at 575°C, following the preliminary anneal (P.A.) at 360°C, results in grain growth, either relatively uniform coalescence of grains or secondary recrystallization during which relatively few grains grow at the expense of many smaller grains. For composition V the specimens which were water quenched from 575°C had grains about 0.06 mm in diameter. The corresponding furnace cooled specimens consisted of only about ten large grains 15–40 mm in diameter. This effect of increased grain growth of furnace cooled specimens as compared with those that were water quenched was also observed to a lesser extent on compositions III and IV.

[1] Manuscript received April 10, 1950. This paper prepared for delivery before the Buffalo Meeting, October 11 to 13, 1950.

[2] Present address: Norwegian Defense Research Establishment, Chemical and Metallurgical Divsion, Lillestrøm, Norway.

[3] Present address: E. I. du Pont de Nemours & Company, Experimental Station, Wilmington, Delaware.

[4] Detailed analyses of some are given in *J.* (*and Trans.*) *Electrochem. Soc.*, **96**, 171 (1949).

UMI

Dissolution Rates

The results of dissolution tests in hydrochloric acid are given in Table I. It is seen that there was a rapid increase in the rate of dissolution as the quantity of impurities in the aluminum increased, especially between compositions II and III. This is in agreement with previous investigators (1, 2). In order to obtain appreciable weight losses for the specimens having low rates, tests as long as 160 hours were made. In those cases where there was intergranular attack, the rates of dissolution given in Table I were determined before any grains dropped out of the surface and, therefore, these high rates are not the result of intergranular disintegration. In every case the specimen which received only the preliminary heat treatment at 360°C had the highest rate of dissolution, and the specimen furnace cooled from 575°C had the lowest rate.

TABLE I. *Effect of heat treatment on the rate of dissolution of aluminum in sodium hydroxide and hydrochloric acid*

Alloy	% Al	Treatment	Rate of dissolution mg/hr 40.5 cm²		Ratio P.A./F.C. or P.A./W.Q.
			in 0.30*N* NaOH at 23°C	in 20% HCl at 25°C	
I	99.998	P.A.	31.2	1.02	—
		W.Q.		0.88	1.2
		F.C.		0.77	1.3
II	99.99	P.A.	116.0	18.7	—
		W.Q.		0.80	21.6
		F.C.		0.74	26.5
III	99.97	P.A.	147.4	1090	—
		W.Q.		204	5.4
		F.C.		37.6	29.2
IV	99.88	P.A.	147.4	6030	—
		W.Q.		1960	3.0
		F.C.		1160	5.7
V	99.57	P.A.	216.7	12100	—
		W.Q.		6950	1.7
		F.C.		5100	2.4
VI	99.2	P.A.	269.1	31200	—
		W.Q.		20600	1.5
		F.C.		20200	1.5

P.A.—preliminary anneal at 360°C.
W.Q.—water quenched from 575°C.
F.C.—furnace cooled from 575°C.

In sodium hydroxide the effect of impurities on the rate of dissolution was much less pronounced. The rate increased from 31.2 to 269.1 mg/hr (40.5 cm²), a factor of about 8, as the impurities increased from composition I to VI. The rates given in Table I are arithmetic averages determined after 4 hours of immersion by dividing the weight loss in mg by the immersion time. The *instantaneous* rate of dissolution of relatively pure aluminum in sodium hydroxide solution increased with immersion time as the impurities in the aluminum accumulated on the surface of the specimen (3). Heat treatment did not affect the rate of dissolution in sodium hydroxide.

The effect of heat treatment on the rate of dissolution in hydrochloric acid may be shown by plotting the ratio of the rate of dissolution of the specimen annealed at 360°C to the rate of dissolution of the specimen heated at 575°C and water quenched (or furnace cooled) against the quantities of impurities (Table I and Fig. 1). Fig. 1 is a plot of the P.A./F.C.[5] ratios. The effect of heat treatment on the rate of dissolution is a maximum for specimens of composition III. With water quenched specimens the maximum effect of heat treatment was obtained with specimens of composition II (Table I). By plotting ratios of dissolution rates only the effect of composition on response to heat treatment is revealed, uninfluenced by absolute dissolution rates.

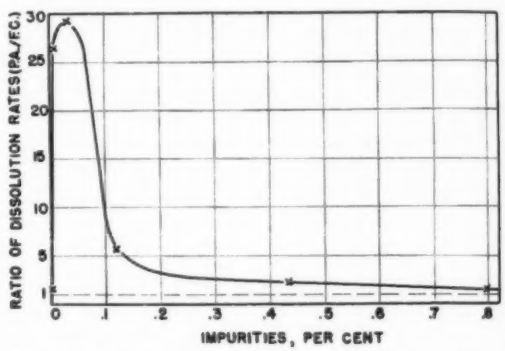

FIG. 1. Effect of heat treatment in changing the rate of dissolution of aluminum with increasing amounts of impurities in 20 per cent HCl at 25°C. The ratio of the dissolution rate of specimens heated only to 360°C (P.A.) to the rate of specimens heated also at 575°C and furnace cooled (F.C.) is plotted against per cent impurities in the metal.

Etch Structures

Fig. 2, 3, 4, and 5 illustrate the elements of the various etch structures produced in hydrochloric acid and sodium hydroxide solutions. The results of metallographic examination are given in Table II. No difference in the type of attack was observed between furnace cooled and water quenched specimens. Specimens of composition II exhibited pronounced intergranular attack in hydrochloric acid, which finally resulted in the dropping out of entire grains

[5] P.A.—rate of dissolution of specimen receiving only preliminary anneal at 360°C; F.C.—rate of dissolution of specimen heated to 575°C and furnace cooled.

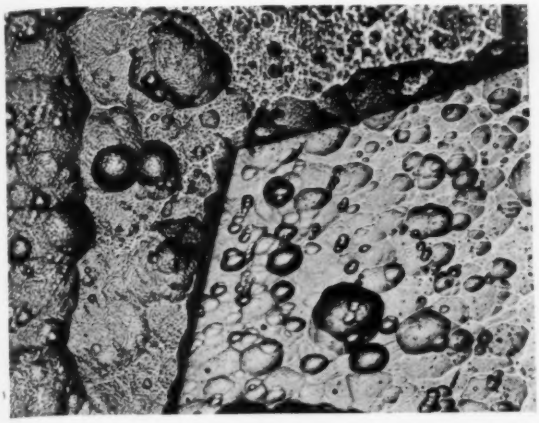

FIG. 2. Composition I (99.998% Al) etched by 0.30*N* NaOH. Step-wise attack (grains dissolve at different rates). Entire surface covered by craters. 250 ×.

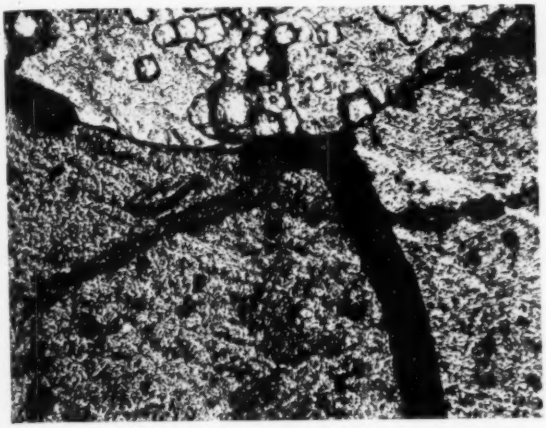

FIG. 3. Composition I (99.998% Al) etched by 20 per cent HCl. Intergranular attack and etch pits. 250 ×.

FIG. 4. Composition III (99.97% Al) etched by 0.30*N* NaOH. V-notch attack at grain boundaries. 250 ×.

after about 10 days of immersion, whereas in sodium hydroxide no intergranular or V-notch attack was observed. With composition III this situation was reversed. In hydrochloric acid there was no intergranular attack, whereas in sodium hydroxide there was a unique type of V-notch attack. The V-notch attack, however, does not lead to undermining of the grains as in the case of the intergranular attack in hydrochloric acid.

FIG. 5. Composition III (99.97% Al) etched by 20 per cent HCl. Angular chasms. Some craters from preliminary etch in NaOH visible. 250 ×.

TABLE II. *Results of metallographic examination of corroded aluminum specimens heat treated at 575°C*

Alloy	Type of attack	
	HCl	NaOH
I	Some intergranular, also step-wise and etch pits	Craters, some V-notch and step-wise
II	Heavier intergranular, deeper pits, also some step-wise,—block structure	Craters, step-wise
III	No intergranular, deep angular chasms,—block structure	Craters, V-notch at grain boundaries
IV	Angular chasms and intergranular,—block structure	Craters, some V-notch, mostly step-wise
V	Angular chasms, no intergranular,—block structure	Craters, all step-wise
VI	Surface covered by adherent black coating	Craters, no grain boundaries visible

Both types of intergranular attack (in hydrochloric acid and sodium hydroxide) do not appear on all grain boundaries. Some boundaries are unattacked probably as a result of almost identical orientation of the two grains forming the boundary as suggested by Lacombe and Yannaquis (4).

For all compositions in sodium hydroxide solutions the grains were covered by merging craters as

a result of attack. In hydrochloric acid a characteristic block structure appeared on specimens of composition II, III, IV, and V. Similar structures on aluminum have been observed by Mahl (19), Mahl and Pawlek (20), and Mahl and Stranski (21).

Fig. 6 shows the block structure produced by hydrochloric acid attack on alloy IV. The acid solution in which alloys II, III, IV, and V dissolved contained a fine powder, which, when filtered and

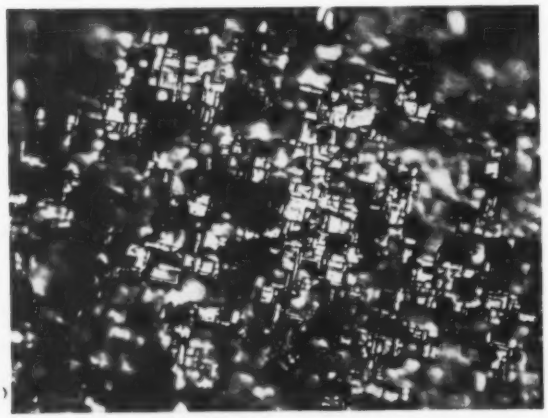

FIG. 6. Composition IV (99.88% Al) etched by HCl. Typical block structure which is also produced on specimens of compositions II, III, and V. 600 ×.

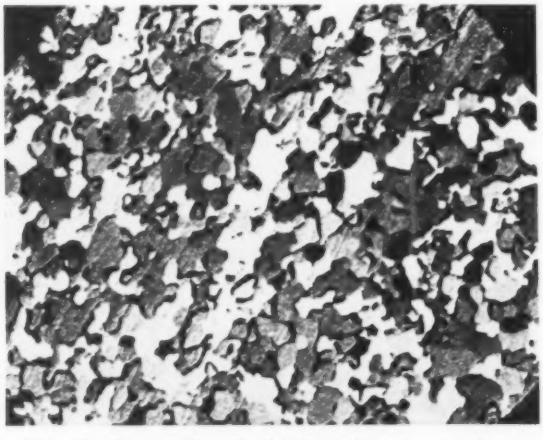

FIG. 7. Composition I (99.998% Al) after prolonged etch in 20 per cent HCl. Black areas indicate where grains have dropped out or where grain boundaries were preferentially attacked to produce perforation. About 2 ×.

examined under the microscope, was found to consist of the same type of rectangular blocks of the order of 0.005 mm as shown in Fig. 6.

When a specimen of composition I, heat treated at 575°C, was allowed to disintegrate almost completely in hydrochloric acid, some grains drop out, and some grain boundaries are corroded through the entire thickness while others remain unattacked (Fig. 7).

DISCUSSION

Dissolution Rates

The main impurities in the aluminum specimens studied were iron, copper, and silicon. Of these, iron was the most effective in accelerating the rate of dissolution of aluminum in both sodium hydroxide and hydrochloric acid (1, 2, 3, 5) by providing cathodes of relatively low overvoltage on the surface of aluminum. The narrow range of composition in which there was an appreciable effect of heat treatment on the rate of dissolution (Fig. 1) suggests that this effect is related to the solubility limits of one of the impurities, probably iron. In a recent determination of the solubility of iron in solid aluminum (6), it was found that the solubility of iron decreases from 0.018 per cent at 575°C to 0.006 per cent at 500°C and less than this at 360°C. The iron content of the specimens I and II was 0.0005 and 0.006 per cent, respectively. It appears likely that the effect of heat treatment on the dissolution rate may be explained by the fact that specimens of compositions I, II, and probably III are solid solutions at 575°C and had a relatively low rate of dissolution. With the exception of I, at 360°C there were two phases present in all specimens including those of composition II and III. Aluminum alloys containing quantities of iron greater than the solubility limit at 575°C (i.e., 0.018% Fe) do not respond to heat treatment to any great extent because they retain the second phase when heated to 575°C. Wiederholt (7) and v. Zeerleder and Zurbrügg (2) observed a similar effect of annealing temperature on the rate of dissolution of aluminum in hydrochloric acid.

It is more difficult to account for the fact that the furnace cooled specimens had a lower rate of dissolution than the water quenched specimens. Furnace cooling might be expected to result in more complete precipitation of second phase than that resulting from water quenching and a higher rate of dissolution as compared with water quenching. Differences in grain size do not appear to be responsible for the differences in dissolution rates between furnace cooled and water quenched specimens. Even water quenching may not have been sufficiently rapid to suppress all precipitation of a second phase. Thus, the corrosion rates of water quenched structures may have been determined by a finely divided precipitate. In the furnace cooled specimens there was probably a greater quantity of precipitate present which had time to agglomerate into fewer and larger particles, resulting in a lower rate of dissolution than the specimens (W.Q.) which contain less, but more finely divided precipitate. In addition the furnace cooled specimens should be in a relatively stress free condition as compared with those that were water quenched and, therefore, the former should have a lower rate.

The absence of any appreciable effect of heat treatment on the rate of dissolution in sodium hydroxide solutions does not speak against an electrochemical mechanism for this process. An increase in impurities in aluminum from 0.002 to 0.8 per cent results in only an 8-fold increase in the rate of dissolution. Thus relatively large quantities of precipitated phase were required to produce an appreciable increase in the rate of dissolution. Apparently the changes in concentration of precipitated phase produced by the heat treatments used were not large enough to affect the rate of dissolution in sodium hydroxide.

In contrast, a very small amount of *iron* deposited by cementation on the surface of aluminum dissolving in sodium hydroxide produced a large increase in the rate of dissolution (8). Thus a small quantity of iron on the surface of aluminum freed when aluminum-iron solid solution dissolves overshadowed the effect of the aluminum-iron compound in increasing the rate of dissolution.

Etch Structures

Previous investigations of the effect of heat treatments on the type of attack on pure aluminum by hydrochloric acid have resulted in apparently contradictory observations. Rohrman (9), using 99.95 per cent aluminum, found that specimens annealed at 600–650°C and quenched from this temperature showed severe intergranular attack in 10–20 per cent hydrochloric acid, dislodging entire grains after 30 days, whereas furnace cooled specimens did not disintegrate intergranularly[6]. However, Lacombe and Yannaquis (11) observed intergranular attack in 10 per cent hydrochloric acid leading to a complete separation of the grains after 25–30 days on specimens of 99.99 and 99.998 per cent Al which had been *furnace cooled* from 600°C after heating 72 hours.

The French investigators (4, 11, 12, 13) have concluded that the etching of the grain boundaries by hydrochloric acid was more influenced by the relative orientations of adjoining crystals than by impurities in the metal itself. The grain boundaries in 99.99 and 99.998 per cent Al were corroded at the same rate in the case of crystals oriented at random, whereas the boundaries separating crystals of nearly identical relative orientations or straight twin boundaries were not corroded at all.

The unique properties of grain boundaries are further revealed by their behavior during melting. Observations of the melting of high purity aluminum in a thermal gradient so that one end was molten while the other remained solid have been made by Chaudron, Lacombe, and Yannaquis (12). It was found that there was a zone where only grain boundaries are molten while twin boundaries remain unaltered[7]. The temperature of incipient melting at grain boundaries in 99.998 per cent Al was found by Pumphrey and Lyons (14) to be 4°C below that of the mass of the metal as determined from the equilibrium diagram.

In the present study no effect of cooling rate on the type of grain boundary attack was observed. This was in apparent contrast to the observations of Rohrman (9) on 99.95 per cent Al. Edwards, in the discussion on Rohrman's paper, indicated that treating aluminum at 600–650°C may result in the formation of some liquid metal[8]. Since the grain boundaries melt at a lower temperature than the grain centers (12, 14), on quenching this phase may be retained as a cast structure in the grain boundaries producing preferential attack. During furnace cooling homogenization of this structure may take place, which may explain the absence of preferential attack at grain boundaries as observed by Rohrman.

Whenever intergranular attack was observed in the present study there were always some grain boundaries which remained unattacked, probably as a result of certain orientation relationships as observed by Lacombe and Yannaquis (4). Inspection of Table II reveals that for a given heat treatment the presence or absence of intergranular attack depends on the composition of the metal. Increasing quantities of impurities may intensify or suppress entirely the intergranular attack.

The type and form of attack was also determined by the corroding solution. There was no intergranular attack of specimens of composition III in hydrochloric acid, but when these specimens were exposed to sodium hydroxide solutions there was an intergranular attack of a unique V-notch type.

The fact that the block structure shown in Fig. 4 appeared on specimens of composition II, III, IV, and V and not on those of composition I, the purest, seems to indicate that this disintegration in the form of blocks was related to the presence of a certain minimum quantity of impurities. Similar block disintegration processes have been observed on arsenic trioxide (15) and Mg_2Sn (16) in distilled water. Traube and Behren (15) concluded that impurities were not responsible for the phenomenon in the case

[6] Electrode potentials measured by Brown (10) in 20 per cent hydrochloric acid on 99.986 per cent Al heated for 1 hour at 620°C and water quenched showed the grain boundaries to be anodic to the grains while on slowly cooled specimens they were cathodic to the grains.

[7] When the metal was heated for 15 hours near the melting point, it was observed in certain cases by these investigators that an inversion of corrosive attack took place. In hydrochloric acid the bulk of the grains dissolved leaving the boundaries uncorroded as a very thin partition.

[8] 99.996 per cent Al melting point: 660.2°C (17).
99.95 per cent Al (0.05% Fe) solidus temperature: 655°C (6)

of arsenic trioxide, while Robertson and Uhlig (16) attribute the splitting of Mg_2Sn into geometric blocks in distilled water (and some other reagents) to hydration of magnesium ions, thus creating local lattice disturbances and attendant stresses that destroy the bond between the (octahedral) planes.

Summary

The effect of heat treatment of aluminum alloys ranging in purity from 99.2 to 99.998 per cent Al on their rates of dissolution and resulting etch structure in hydrochloric acid and in sodium hydroxide solutions has been studied. The specimens were process annealed at 360°C and some were then heated at 575°C. From the high temperature one half of the specimens were water quenched and the remaining half were allowed to furnace cool.

1. Larger grain size resulted with specimens of compositions II, IV, and V which were furnace cooled from 575°C than with specimens which were water quenched from this temperature.

2. When the impurities in aluminum were increased from 0.002 per cent to 0.8 per cent, the change in rate of dissolution in sodium hydroxide was relatively small, (an 8-fold increase) while in hydrochloric acid there was a 30,000 fold increase.

3. Heat treatments had no effect on the rate of dissolution in sodium hydroxide, but this fact does not conflict with an electrochemical interpretation of this process because relatively large changes in concentration of impurities in aluminum were required to bring about appreciable changes in dissolution rates.

4. Corrosion rate data from hydrochloric acid tests revealed that heat treatments were most effective in a narrow range of impurity (iron) content, indicating that a change in solid solubility with temperature of heating was involved.

5. Intergranular attack on aluminum appears to be determined by:

(*a*) the composition of the metal (type and quantity of impurities)

(*b*) the heat treatment cycle to which the metal was subjected. The rate of cooling apparently did not affect the type of attack unless the metal was partially melted during heating.

(*c*) the type of corroding solution. A given specimen may have been attacked intergranularly in hydrochloric acid and suffer only general attack in sodium hydroxide and vice versa.

(*d*) the orientation of grains in relation to each other as suggested by Lacombe and Yannaquis (4).

6. In sodium hydroxide a unique form of intergranular attack of a V-notch type was observed.

7. When specimens of composition II, III, IV, and V dissolved in hydrochloric acid, a fine dust was found in the solution which consists of rectangular blocks of the order of 0.005 mm in length, similar in structure to that observed on the surface of the metal. Highest purity aluminum (99.998% Al) did not develop a block structure in hydrochloric acid.

Acknowledgment

The authors wish to thank Dr. Walter Beck, Director of the Corrosion Research Laboratory, Lehigh University, for having made this investigation possible; the Signal Corps Engineering Laboratories, Fort Monmouth, New Jersey, for permission to publish the results of this study; and Dr. E. M. Mahla, E. I. du Pont de Nemours & Company, for discussion and suggestions. The authors are indebted to Dr. W. Rostoker, University of Birmingham, England; Dr. H. P. Godard, Aluminum Laboratories, Ltd., Kingston, Ontario; and Mr. E. D. Verink, Jr., Aluminum Company of America, New Kensington, Pennsylvania, for the aluminum used in this investigation.

Any discussion of this paper will appear in a Discussion Section, to be published in the June 1951 issue of the Journal.

REFERENCES

1. M. Straumanis, *Korrosion u. Metallschutz*, **14,** 1 (1938).
2. A. v. Zeerleder and E. Zurbrügg, *Aluminium*, **20,** 365 (1938).
3. M. A. Streicher, *J. (and. Trans.) Electrochem. Soc.*, **93,** 285 (1948).
4. P. Lacombe and L. Beaujard, *J. Inst. Metals*, **74,** 1 (1947).
   N. Yannaquis and P. Lacombe, *Compt. rend.*, **226,** 498 (1948).
   G. Chaudron, *Helv. Chim Acta*, **31,** 1553 (1948).
5. M. Straumanis and N. Brakšs, *Korrosion u. Metallschutz*, **15,** 5 (1939).
6. J. K. Edgar, *Am. Inst. Mining Met. Engrs. Tech. Pub.*, No. 2389 (June 1948).
7. W. Wiederholt, *Z. anorg. u. allgem. Chem.*, **154,** 226 (1926).
8. M. A. Streicher, *J. (and Trans.) Electrochem. Soc.*, **96,** 170 (1949).
9. F. A. Rohrman, *Trans. Electrochem. Soc.*, **66,** 229 (1934).
10. R. B. Mears and R. H. Brown, *Ind. Eng. Chem.*, **33,** 1001 (1941).
11. P. Lacombe and N. Yannaquis, *Rev. mét.*, **45,** 68 (1948).
12. G. Chaudron, P. Lacombe, and N. Yannaquis, *Nature*, **162,** 854 (1948).
13. P. Lacombe, "Physical Society Bristol Conference Report," p. 91, London (1948).
14. W. I. Pumphrey and J. V. Lyons, *Nature*, **163,** 960 (1949).

15. J. Traube and W. V. Behren, *Z. physik. Chem.*, **138,** 85 (1928); see also W. Hume-Rothery, "The Structure of Metals and Alloys," p. 128, Institute of Metals, London (1945).
16. W. D. Robertson and H. H. Uhlig, *J. (and Trans.) Electrochem. Soc.*, **96,** 27 (1949).
17. "Metals Handbook," p. 810, A. S. M., Cleveland, Ohio (1948).
18. M. Schenk, "Werkstoff Aluminium und seine anodische Oxydation," pp. 363-66 and 478, A. Francke Ag. Verlag, Bern (1948).
19. H. Mahl, *Metallwirtschaft*, **29,** 1082 (1940).
20. H. Mahl and F. Pawlek, *Z. Metallkunde*, **34,** 232 (1942).
21. H. Mahl and I. N. Stranski, *Naturwissenschaften*, **31,** 12 (1943).

The Rate of Corrosion of Silver in Solutions of Ferric Sulfate[1]

HUGH SALZBERG AND CECIL V. KING

Department of Chemistry, New York University, New York, N. Y.

ABSTRACT

Metals down to copper in the emf series dissolve in ferric salt solutions at maximum, diffusion controlled rates, with quantitative reduction of ferric to ferrous ion. Silver, however, reaches an equilibrium with only partial reduction of ferric ion, and the dissolution rate is smaller than with more active metals.

This paper reports a study of the corrosion or dissolution rate of silver in ferric salt solutions as a function of (*a*) the concentration of the ions involved, (*b*) the concentration of the acid, (*c*) speed of stirring, (*d*) temperature, and (*e*) emf of the silver-silver ion, ferric-ferrous ion cell. The rate has been found to be greatly influenced by adsorption of ions formed in the reaction. A rate equation has been derived which includes the effects of adsorption and of the reverse reaction.

INTRODUCTION

Van Name and Hill (1) found that zinc, cadmium, iron, nickel, and tin dissolve at approximately the same rate in ferric alum solutions containing sulfuric acid. They postulated a diffusion controlled rate in these cases, in accordance with the theory of Nernst. Copper, they found, dissolves at almost the same rate, but silver dissolves much more slowly and the rate is decreased by the silver ion formed or by added silver sulfate. Van Name and Hill point out that a slow chemical reaction may lead to a rate in which diffusion speed plays no part, and that intermediate rates are also possible.

This paper presents the results of a study of the rate of dissolution of silver in dilute ferric salt solutions, chiefly ferric sulfate, with sufficient acid to repress hydrolysis and with added ferrous and silver sulfates to bring the system near equilibrium. As equilibrium is approached

$$Ag + Fe^{+++} \rightleftarrows Ag^{+} + Fe^{++} \qquad (I)$$

it is to be expected that the rate of the reverse reaction will approach that of the forward reaction and the net rate will decrease to zero.

Preliminary experiments with sterling silver (approximately 8 per cent copper) in ferric nitrate solutions (2) showed that the dissolution rate decreased with time far faster than was to be expected from known values of the equilibrium constant. The purpose of this work was to study the factors which affect the net reaction rate. The metal silver and the oxidizing agent ferric ion were chosen because the normal potentials of the silver-silver ion and ferric-ferrous ion pairs are close together and it was desired to learn whether low rates are caused directly by low potential differences.

EXPERIMENTAL PROCEDURE

Cylinders of pure silver were prepared, approximately 1.5 cm in diameter and 2 cm long. These were mounted on a steel motor-driven shaft with the ends protected by sulfur-free rubber washers; the remainder of the shaft was protected by a close-fitting bakelite sleeve. The cylinders were rotated in 500 ml of solution and the speed of rotation was measured with a stroboscopic counter which had been calibrated with a synchronous motor.

The temperature of the solution was controlled within ± 0.2°C. Potentials were measured with a student type potentiometer. Contact with the silver was made through a mercury cup mounted at the top of the motor shaft, and a platinum electrode was immersed in the solution to respond to the ferric-ferrous ion potential.

Stock solutions of ferric sulfate were prepared, containing enough sulfuric acid to give clear solutions, and standardized with the aid of a Jones reductor and permanganate titration. In some experiments, weighed amounts of anhydrous ferrous sulfate were dissolved in the solutions; in others, aliquot portions of freshly prepared stock solutions containing sulfuric acid were added.

The rates were measured by weighing the silver cylinders before and after each run. Each cylinder weighed approximately 30 grams and was weighed to 0.1 mg. When rotated in water and dried with filter paper, the weight checked to ± 0.1 mg. When rotated in the various solutions used for two to ten minutes, the weight loss could be duplicated, as a rule, within

[1] Manuscript received February 24, 1950. This paper, from a thesis submitted by Hugh Salzberg to the Graduate School of New York University in partial fulfillment of the requirements for the degree Doctor of Philosophy, prepared for delivery before the Buffalo Meeting, October 11 to 13, 1950.

±0.3 mg., the precision being almost independent of the actual amount dissolved.

Experimental Results

Time of each run.—In most of the solutions used it was found that the reagent concentrations did not change appreciably in the first 15 minutes or more. Successive two-minute runs could be made in ferric sulfate solutions with little change in rate. In ferric nitrate or perchlorate solutions, however, the rate fell off rapidly during the first few minutes, although extrapolation to zero time gives values similar to those obtained in the sulfate solution. Fig. 1 shows typical results.

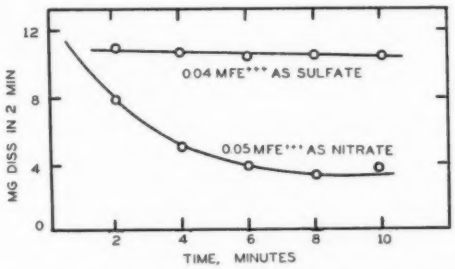

Fig. 1. The dissolution rate of silver in ferric sulfate and ferric nitrate. 30°C, 4000 rpm or 304 cm/sec peripheral speed.

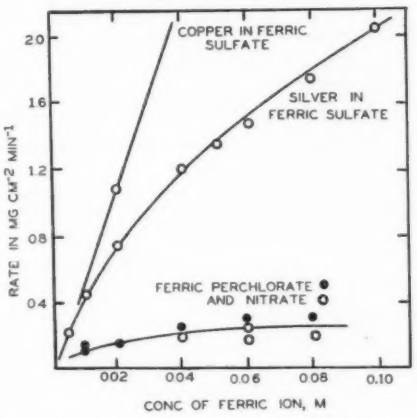

Fig. 2. The effect of anions and comparison with diffusion control. 4000 rpm, 30°C. The dissolution rate of a copper cylinder at the same temperature and peripheral speed is given in terms of mg silver per cm² per min.

Surface condition.—Where corrosion rates were relatively high as in the absence of reaction products, it was found that the rates were nearly independent of the preliminary surface treatment, i.e., etching with various reagents, polishing with fine emery or rouge papers or electropolishing.

With near-equilibrium concentrations the rates are comparatively low and varied a great deal with the surface treatment. For example, when the cylinder was first brought to a high polish with rouge paper, the rate fell off steadily in successive two-minute runs although the concentrations of reagents were hardly changed. Upon repolishing twice, with removal of less than one mg of silver each time, the rate rose to the initial value.

Since the rates were more reproducible with polished cylinders and were easier to measure because of the higher values, the cylinders were always polished between runs. In spite of these advantages, this procedure has two obvious disadvantages: (*a*) the rates so obtained are from a special cold-worked and abraded layer of silver rather than from natural crystalline faces, and (*b*) not more than 5 or 6 mg could be dissolved in any one experiment without weighing and repolishing the cylinder. These comments apply only to slow rates in near-equilibrium solutions.

In all the figures and tables of this paper except Fig. 1, rates are reported as milligrams silver dissolving per square centimeter surface per minute. The actual amounts dissolved per run varied from a maximum of about 60 mg per two minute run in 0.08*M* ferric ion solutions (as sulfate) to a minimum of 3 or 4 mg in ten minute runs in near-equilibrium solutions. The maximum amount of ferric ion reduced in any one run was about two per cent of the amount present in the 500 ml of solution used. The rates reported are considered as "instantaneous" values and are equivalent to dx/dt in the usual rate equations.

Anions.—Curve 2 of Fig. 1 is similar to curves found by Reass (2), using sterling silver and ferric nitrate, and shows that the decrease in rate is caused by the anion and not by the copper content of the sterling silver. Fig. 2 shows that the solution rates in ferric nitrate and ferric perchlorate solutions are lower at all concentrations than in ferric sulfate, and nearly independent of the concentration. These are rates measured after a few minutes and correspond to the flat portion of curve 2, Fig. 1.

All further experiments were carried out with ferric sulfate and sulfuric acid.

Comparison with diffusion controlled rates.—If the rates in ferric sulfate were entirely diffusion controlled, they should be proportional to the ferric ion concentration and should coincide approximately with the straight line (curve 1) of Fig. 2. This line was obtained by rotating a copper cylinder at the same peripheral speed in solutions of the same concentration and temperature. Points at higher concentrations than the one shown in the plot give the same slope. The amount dissolved was calculated in terms of mg silver. The rates in equivalents per minute are almost the same as has been found at 25°C for iron in ferric chloride (3) and copper at

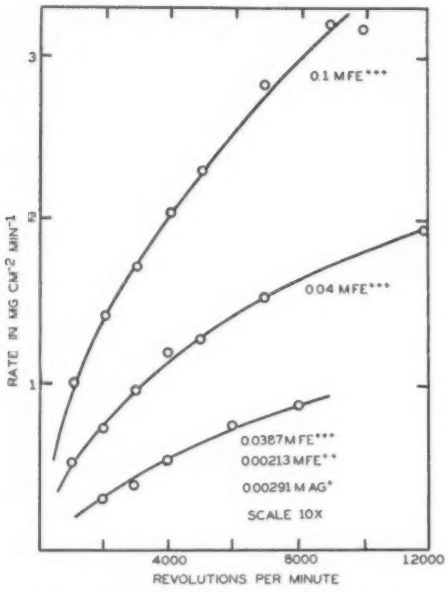

FIG. 3. The dissolution rate of silver at 30°C vs. rotational speed. 4000 rpm correspond to a peripheral speed of 304 cm/sec.

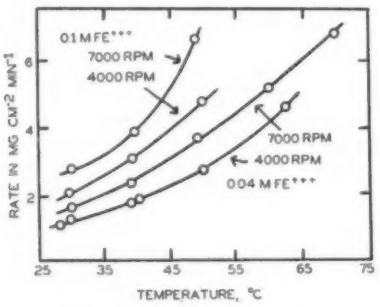

FIG. 4. Temperature coefficient, silver in ferric sulfate

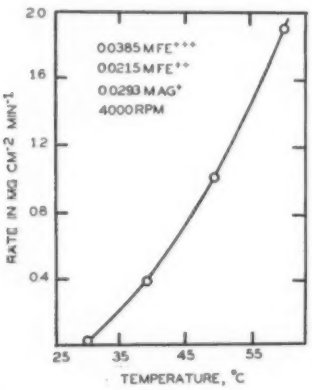

FIG. 5. Temperature coefficient in a solution near equilibrium at 30°C.

25°C in ferric chloride or nitrate (4) from cylinders rotated at the same peripheral speed.

It is evident that in very dilute ferric sulfate silver dissolves at a rate approaching that of diffusion control, and that another factor is of increasing importance at higher concentrations.

Acid concentration.—Hydrogen ion does not enter the reaction directly and was added only to minimize hydrolysis of the salts. A series of 15 runs with 0.005*M* ferric ion and sulfuric acid between 0.05*N* and 0.3*N* gave the same rate within experimental error. In all other runs including those previously described the acid concentration was kept at approximately 0.3*N*.

Salt effect.—Since sulfuric acid has so little effect on the rate we may assume that general salt effect is negligible. However, a series of runs was made with zinc sulfate up to 0.14*M* added to 0.04*M* ferric ion (as sulfate) with 0.3*N* sulfuric acid. The effect was to decrease the rate a total of 17 per cent, nearly linearly with the concentration; the rate was reduced from 1.20 to 1.00 mg cm^{-2} min^{-1}. This is probably a specific effect of the zinc ion, but is much smaller than the effect of ferrous and silver ions to be described below.

Rotational speed.—The effect of changing the speed of rotation of the silver cylinders is shown in Fig. 3. Diffusion controlled rates are linear with rpm or peripheral speed above a few thousand cm/min (5), whereas chemically controlled rates are probably independent of stirring speed. Some influence of rotational speed was found in all experiments, even in solutions very near the equilibrium point (as shown in Table I).

Temperature coefficients.—Fig. 4 and 5 show the effect of temperature on the rates in solutions of two quite different types. With no reaction product initially present and very little formed in the runs (Fig. 5), the average temperature coefficient is about 1.5 per 10°C, which indicates a considerable degree of diffusion control. On the other hand, in a solution which is very near equilibrium at 30°C (Fig. 5) the temperature effect is much greater and the coefficient changes rapidly with temperature.

Ferrous and silver ions.—Added ferrous and silver sulfates decrease the rate far more than zinc sulfate, as shown in Fig. 6 and 7. Silver ion has a greater effect than ferrous ion, at the same concentration. Each has a large effect even though the other is absent or present in negligible concentration. This is not in accord with a simple reversible system with a back reaction rate proportional to the product of these two concentrations. Furthermore, a plot of rate vs. the product $C_{Ag^+}C_{Fe^{++}}$ gives a series of curves for each constant value of either ion as the concentration of the other is varied.

Rate and emf.—The emf between silver cylinder and platinum electrode was independent of rota-

tional speed in systems far from equilibrium, although the rate of dissolution always increased with increasing speed. Further, the emf might decrease several millivolts during a two-minute run, although several successive runs gave almost identical solution rates.

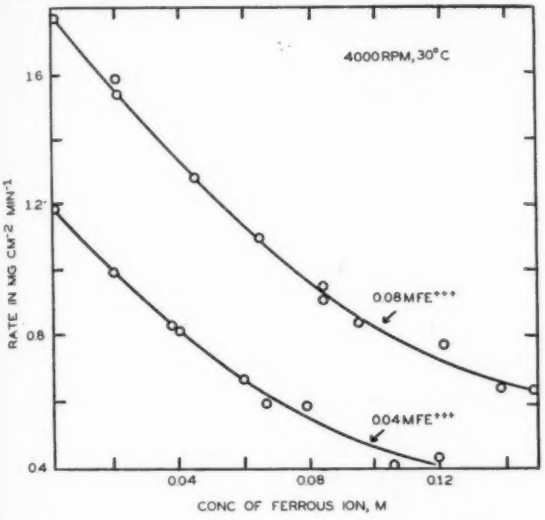

FIG. 6. The effect of ferrous sulfate on the dissolution rate of silver in ferric sulfate.

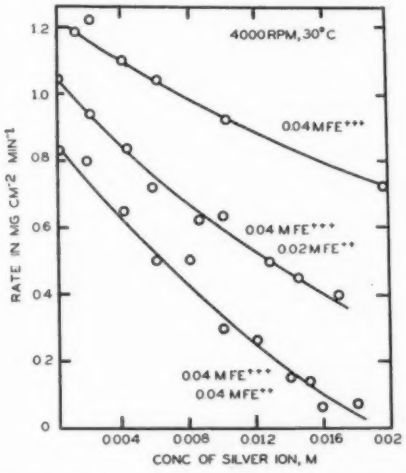

FIG. 7. The effect of silver sulfate on the dissolution rate of silver in ferric sulfate.

At near-equilibrium conditions the emf always decreased by 0.5 to 2 mv when rotation was started and there was no obvious relation between emf and rate. Typical results are given in Table I. The experiments were successive two-minute runs in the same solution.

The experiments shown in Fig. 8 were run to observe the relation between emf and rate over a wide range of concentrations. Solutions of ferric sulfate were prepared as indicated, and ferrous and silver sulfates were added to bring the emf to the values shown. While, in general, the rates decrease as the emf decreases, the two are obviously dependent on quite different functions of the ion concentrations.

The following experiment gives concrete evidence of the reverse reaction. To several solutions very near equilibrium (as the one described in Table I) a few drops of ferrous or silver sulfate were added so that very small shiny silver crystals appeared throughout the solution. On rotating a silver cylinder in this solution for long periods, it gained in weight at the rate of about one milligram per hour. Presumably the small crystals dissolve slowly while silver deposits on the cylinder. Supersaturated solutions could not be prepared.

TABLE I. *Rate, emf, and rotational speed*
$0.04M$ Fe^{+++}, $0.0654M$ Fe^{++}, $0.0085M$ Ag^{+}, 30°C

rpm	emf, mv	R, mg cm^{-2} min^{-1}
0	3.5	negligible
4000	1.2	0.206
8000	1.3	0.518
0	2.6	0.052
4000	0.85	0.232
8000	0.95	0.362

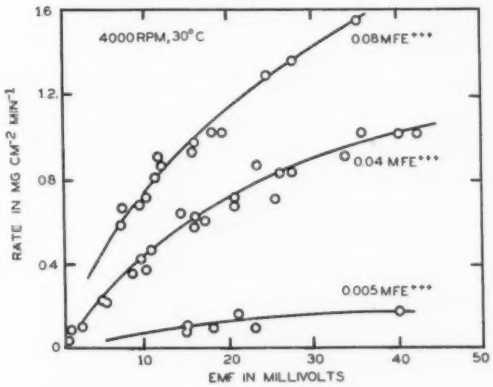

FIG. 8. The dissolution rate vs. potential between silver and a platinum electrode. Various amounts of ferrous and silver sulfates were added to obtain the potentials shown.

INTERPRETATION OF RESULTS

The curvature of the plot of rate vs. ferric ion concentration, the strong inhibiting effect of ferrous and silver ions and the lack of proportionality of this effect to the product of the ion concentrations indicate that all these ions are adsorbed on the silver surface and thus influence the rate.

An equation describing all features of the observed rates may be derived on the basis of the following assumptions: (*a*) The net rate is the difference be-

tween a forward and a reverse rate and both are affected by adsorption. (*b*) The adsorption of each ion follows the form of a Langmuir isotherm except that, as shown in the equations below, equilibrium is not maintained while dissolution is proceeding. (*c*) The forward rate is proportional to the amount of ferric ion adsorbed. (*d*) The reverse reaction occurs when a free ferrous ion collides with an adsorbed silver ion, or vice versa. (*e*) The surface area covered by adsorbed ferric ions is small compared to the area covered by ferrous and silver ions, when these ions are present in appreciable concentrations.

These postulates may be put in the following form: Let θ_1, θ_2, θ_3 be the fraction of silver surface covered by Ag^+, Fe^{++}, and Fe^{+++} ions respectively, and c_1, c_2, c_3 be concentrations of the same ions. R is the net reaction rate in any convenient units, as mg cm^{-2} min^{-1}. The surface areas which would normally be covered by silver and ferrous ions are increased by factors proportional to R, since these ions are continually being formed, while the area normally covered by ferric ion is diminished by a similar factor since this ion is being reduced to ferrous ion. Then

$$\theta_1 = a_1c_1(1 - \theta) + a'R \quad \text{(II)}$$
$$\theta_2 = a_2c_2(1 - \theta) + a''R \quad \text{(III)}$$
$$\theta_3 = a_3c_3(1 - \theta) - a'''R \quad \text{(IV)}$$
$$\theta = \theta_1 + \theta_2 \quad \text{(V)}$$

The a's are constants of the isotherms. The rate equation is

$$R = k\theta_3 - k'c_1\theta_2 - k''c_2\theta_1 \quad \text{(VI)}$$

where the k's are constants.

Simultaneous solution of equations (II) to (VI) leads to the final rate equation

$$R = \frac{k_1c_3 - k_2c_1c_2}{1 + k_3c_3 + k_4c_1 + k_5c_1^2 + k_6c_2 + k_7c_2^2 - k_8c_1c_2}, \quad \text{(VII)}$$

where k_1 to k_8 replace all the other constants. Equation (VII) may be applied to the data and numerical values of the constants may be found as shown below.

Application of Rate Equation

1. Rates in ferric sulfate alone.—Considering the concentration of ferrous and silver ions to be negligible, equation (VII) reduces to

$$R = \frac{k_1c_3}{1 + k_3c_3} \quad \text{(VIII)}$$

While equation (VIII) does not follow directly from assumption (*e*) in the preceding section, it may be derived independently by postulating that, in the absence of silver and ferrous ions,

$$R = k\theta_3 \text{ and } \theta_3 = a_3c_3(1 - \theta_3).$$

By inverting (VIII) an equation which is linear in $1/R$ and $1/c_3$ results:

$$1/R = (1/k_1)(1/c_3) + k_3/k_1 \quad \text{(IX)}$$

The data shown in curve 2 of Fig. 3 were plotted as reciprocals and the constants determined: $k_1 = 46.7$, $k_3 = 14.0$. Table II compares the experimental rates with values calculated from equation (VIII).

TABLE II. *Solution rates in ferric sulfate solutions* 4000 rpm or 304 cm/sec, 30°C

$C_{Fe^{+++}}$, *M*	*R*, observed	*R*, calculated
	mg cm⁻²min⁻¹	
0.005	0.216	0.218
0.01	0.44	0.410
0.02	0.73	0.732
0.04	1.20	1.20
0.05	1.37	1.37
0.06	1.47	1.52
0.08	1.73	1.76
0.10	2.04	1.95
Average difference		0.0255

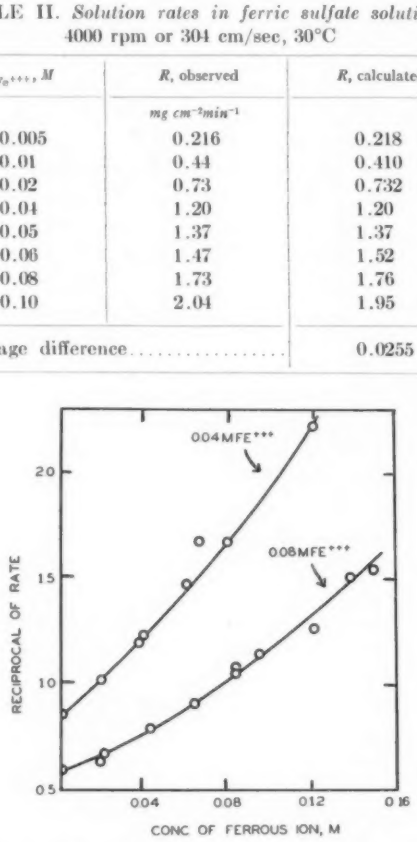

FIG. 9. Reciprocal of the rate vs. ferrous ion concentration. Data of Fig. 6, 4000 rpm, 30°C.

2. The effect of ferrous ion.—In the experiments of Fig. 6, ferric ion was present in constant concentrations and the amount of silver ion was negligible. Under these conditions equation (VII) may be put in the form:

$$\frac{1}{R} - \frac{1 + k_3c_3}{k_1c_3} = \frac{k_6}{k_1c_3} \cdot c_2 + \frac{k_7}{k_1c_3} \cdot c_2^2 \quad \text{(X)}$$

The curvature of the plots of $1/R$ vs. c_2 in Fig. 9 shows the necessity of the c_2^2 term in equation (X).

By plotting the left side of (X) divided by c_2, vs. c_2, the constants k_6 and k_7 may be evaluated. While points on such a plot are somewhat scattered since experimental errors are magnified, average values were chosen as follows: $k_6 = 13.5$, $k_7 = 90$. Table III compares the experimental rates with values calculated from equation (VII).

3. The effect of silver ion.—With constant ferric ion concentration and negligible ferrous ion, the effect of silver ion may be analyzed as above. This method applies to curve 1 of Fig. 7, and suitable

TABLE III. *The effect of ferrous sulfate on the solution rates*
4000 rpm or 304 cm/sec, 30°C

0.04*M* Fe^{+++}			0.08*M* Fe^{+++}		
$C_{Fe^{++}}$, *M*	*R*, observed	*R*, calculated	$C_{Fe^{++}}$, *M*	*R*, observed	*R*, calculated
0	1.20	1.20	0	1.73	1.76
0.0189	1.00	1.01	0.0201	1.59	1.54
0.02	1.03	1.00	0.0206	1.54	1.53
0.0379	0.84	0.845	0.0432	1.29	1.29
0.04	0.82	0.83	0.0636	1.11	1.12
0.06	0.63	0.69	0.0835	0.965	0.96
0.0665	0.60	0.66	0.0838	0.925	0.96
0.08	0.60	0.58	0.0950	0.85	0.89
0.106	0.41	0.46	0.121	0.79	0.77
0.12	0.45	0.42	0.139	0.67	0.65
			0.149	0.55	0.61
Average difference		0.0275	Average difference		0.0255

TABLE IV. *The effect of silver sulfate on the solution rates*
0.04*M* Fe^{+++}, no Fe^{++}. 4000 rpm, 30°C

C_{Ag^+}, *M*	*R*, observed	*R*, calculated
0	1.20	1.20
0.001	1.18	1.18
0.002	1.22	1.14
0.004	1.09	1.09
0.006	1.04	1.03
0.01	0.92	0.93
0.02	0.715	0.71
Average difference		0.0150

values of the constants are: $k_4 = 35.5$, $k_5 = 930$. In Table IV the experimental rates are compared with calculated values.

4. The effect of ferrous and silver ions together.—When both these ions are present the terms in c_1c_2 can no longer be ignored, and the constants k_2 and k_8 must be evaluated. Equation (VII) may be rearranged as follows:

$$\frac{R(1 + k_3c_3 + k_4c_1 + k_5c_1^2 + k_6c_2 + k_7c_2^2) - k_1c_3}{c_1c_2} = k_8R - k_2 \quad \text{(XI)}$$

A plot of the left member of equation (XI) vs. R should be linear. All available data (curves 2 and 3 of Fig. 7) are plotted in this manner in Fig. 10. It is obvious that k_8 is neglgible; 2500 is chosen as the best value of k_2.

Table V compares the measured rates in these experiments with values calculated from equation (VII).

A summary of the constants of equation (VII) with their units follows. These values are for a rotational speed of 4000 rpm with the cylinders used, or 304 cm/sec peripheral speed, and 30°C.

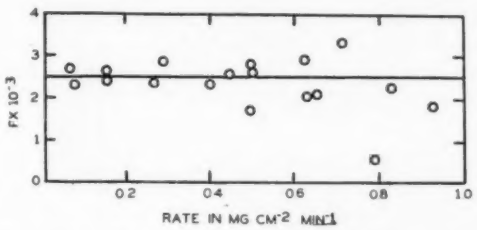

FIG. 10. A plot of F, the left side of equation (XI), vs. rate.

TABLE V. *The effect of ferrous and silver ions together on the solution rates*
4000 rpm, 30°C, 0.04*M* Fe^{+++}

0.02*M* Fe^{++}			0.04 *M* Fe^{++}		
C_{Ag^+}, *M*	*R*, observed	*R*, calculated	C_{Ag^+}, *M*	*R*, observed	*R*, calculated
0	1.03	1.00	0	0.82	0.83
0.00191	0.93	0.92	0.00182	0.79	0.73
0.00423	0.83	0.81	0.00396	0.65	0.61
0.00574	0.71	0.75	0.0060	0.495	0.52
0.0085	0.62	0.65	0.0080	0.495	0.413
0.0100	0.63	0.60	0.010	0.289	0.322
0.0127	0.495	0.492	0.012	0.263	0.238
0.0144	0.446	0.447	0.014	0.150	0.160
0.0169	0.395	0.375	0.015	0.148	0.123
			0.016	0.061	0.088
			0.018	0.070	0.021
Average difference		0.0204	Average difference		0.0351

$k_1 = 46.7$ mg liters moles^{-1} cm^{-2} min^{-1}
$k_2 = 2500$ mg liters^2 moles^{-2} cm^{-2} min^{-1}
$k_3 = 14.0$ liters moles^{-1}
$k_4 = 35.5$ liters moles^{-1}
$k_5 = 930$ liters^2 moles^{-2}
$k_6 = 13.5$ liters moles^{-1}
$k_7 = 90$ liters^2 moles^{-2}
$k_8 = 0$ liters^2 moles^{-2}

DISCUSSION

It is evident that equation (VII) gives excellent agreement with the experimental data with the ex-

ception of a few scattered points. Almost equally good agreement is obtained by omitting the terms $k_2c_1^2$ and $k_3c_1c_2$, which were introduced to account for a slight curvature of the plot of $1/R$ vs. C_{Ag^+} for the data of Table IV. Additional data are needed to tell whether this curvature is real or not. The simpler equation is derived by omitting the term $a''R$ from equation (III) and the term $k'c_1\theta_2$ from equation (VI). This amounts to assuming either that free silver ion does not react with adsorbed ferrous ion, or that silver so formed is not deposited on the cylinder.

The constant k_1 purports to give the rate in the absence of all adsorption and might be expected to agree with the constant for the diffusion controlled rate with copper. The value of the latter, from the slope of the straight line in Fig. 2, is 55.5 in the same units, compared to $k_1 = 46.7$. The discrepancy may be explained either by a finite though short life of adsorbed ferric ion before reduction, or by some degree of error in the assumption that the amounts of ferrous and silver ion formed are negligible in the two minute runs used to establish curve 2 of Fig. 2.

If it may be assumed that the entire silver surface acquires a positive charge from adsorbed ions as soon as dissolution begins, an explanation is available for the lower rates in nitrate and perchlorate solutions. A sulfato-ferric ion, of negative or reduced positive charge, can be adsorbed and react more readily than a triply positive (hydrated) ferric ion. While no data are available as to the extent of complex formation between ferric and sulfate ion it is thought that many polyvalent metal ions do form such complexes because their transport numbers become small or negative in the presence of sulfates (6). Ceric ion has been reported to exist as a negative complex in sulfuric acid solutions (7). The change in color of ferric nitrate solutions on adding nitric acid, and the ultraviolet absorption of ferric perchlorate solutions (8), indicate that these ions do not form complexes.

A few experiments not reported above showed that addition of sulfuric acid or potassium sulfate to ferric nitrate or perchlorate increases the rate considerably, while addition of nitric or perchloric acids to ferric sulfate does not decrease the rate much.

While it has long been assumed that metal ions are adsorbed from salt solutions by metals, little direct experimental evidence is available. Work with radioactive tracers has shown that metals *exchange* atoms with their own and other metallic ions in solution and that the rate of exchange is influenced by the anions present (9). The speed and extent of exchange between silver and silver ion has been measured (10, 11). The process apparently involves local cell action on the silver surface, with considerable dissolution taking place at anodic areas and corresponding deposition occurring at cathodic areas.

Although such experiments do not prove that these ions are adsorbed it is probable that adsorption accompanies the exchange. It has been reported that considerable radioactive sodium ion is removed by silver from sodium carbonate solution (12), but the experiment seems open to question. The data of this paper indicate that silver ion is strongly adsorbed on silver, ferrous ion to a lesser extent; zinc ion is probably weakly adsorbed while sulfuric acid and potassium sulfate give no evidence of adsorption.

We must conclude from the above experimental data that the relative potentials of oxidant and reductant have only indirect connection with reaction rates in the sulfate solutions. The system is not self-polarizing in the electrical sense; the sulfato-ferric ion reacts almost instantly provided it finds a vacant spot on the silver surface. The reaction rate is limited by three factors: (*a*) diffusion speed, effective with very dilute ferric ion in the absence of corrosion products; (*b*) the fraction of uncovered surface; and (*c*) the reverse reaction. With nitrate or perchlorate solutions and unpolished silver surfaces the conclusions might be different.

An analogous reaction of quite different behavior is that of aluminum in ceric-cerous sulfates in sulfuric acid, studied by Petrocelli (13). Here the normal potentials differ by some 3 volts and the reverse reaction is entirely negligible. The dissolution rate is very low because of interference by an oxide film on the metal and within wide limits is independent of the concentrations of ceric, cerous or aluminum ions.

For reactions in homogeneous solution it has been shown that oxidation-reduction potentials are related to rates only in special cases. These have been summarized and discussed by Remick (14). In one such case the potential is determined by an equilibrium which involves a molecule or ion whose concentration is rate controlling. In another case, the reaction procedes over an energy barrier which makes it essentially nonreversible, and the potential required for appreciable rates is higher than the calculated reversible potential of the system. The latter case no doubt has analogies in heterogeneous reactions including metal corrosion.

There is good reason to believe that the forward and reverse reactions continue at equilibrium with silver in ferric-ferrous-silver ion systems, even though the potential difference is zero. In fact the two rates can be calculated separately by separating the right side of equation (VII) into its two component terms. It has long been assumed that the equilibrium state is a dynamic one and work with radioactive tracers has made it possible to verify this. For example higher and lower valence states of certain ions may

exchange electrons rapidly even though the initial and final states have no difference in potential (15).

The fact that the rotational speed of the cylinders affects the corrosion rate in all the solutions used indicates either that concentration gradients exist at the silver surface or that the speed of the adsorption processes are affected by the rotation. The assumptions made in equations (II), (III), and (IV) that the amount of each ion adsorbed depends on its bulk concentration *and* the rate, are possibly required because concentration gradients do exist at the surface.

Any discussion of this paper will appear in a Discussion Section, to be published in the June 1951 issue of the JOURNAL.

REFERENCES

1. E. A. VAN NAME AND D. V. HILL, *Am. J. Sci.* (4), **42,** 307 (1916).
2. C. A. REASS, Master's Thesis, New York University (1948).
3. M. B. ABRAMSON AND C. V. KING, *J. Am. Chem. Soc.*, **61,** 2290 (1939).
4. C. V. KING AND L. WEIDENHAMMER, *J. Am. Chem. Soc.*, **58,** 602 (1936).
5. C. V. KING AND M. SCHACK, *J. Am. Chem. Soc.*, **57,** 1212 (1935).
6. J. W. MCBAIN AND P. J. VAN RYSSELBERGHE, *J. Am. Chem. Soc.*, **50,** 3009 (1928).
7. G. F. SMITH AND G. A. GETZ, *Ind. Eng. Chem. Anal. Ed.*, **10,** 191 (1938).
8. A. R. OLSON AND T. R. SIMONSON, *J. Chem. Phys.*, **17,** 1322 (1949).
9. M. HAISSINSKY, M. COTTIN, AND B. VARJABEDIAN, *J. chim. phys.*, **45,** 212 (1948).
10. B. V. ROLLIN, *J. Am. Chem. Soc.*, **62,** 86 (1940).
11. C. C. COFFIN AND I. I. TINGLEY, *J. Chem. Phys.*, **17,** 502 (1949).
12. J. W. HENSLEY, A. O. LONG, AND J. E. WILLARD, *Ind. Eng. Chem.*, **41,** 1415 (1949).
13. J. V. PETROCELLI, *J. Electrochem. Soc.*, **97,** 10 (1950).
14. A. E. REMICK, "Electronic Interpretations of Organic Chemistry," 2nd Ed., p. 569. John Wiley & Sons, Inc., New York (1949).
15. J. W. GRYDER, *Trans. N. Y. Acad. Sci.* (*II*), **12,** 18 (1949).

THE ELECTROCHEMICAL SOCIETY, INC.

The Electrochemical Society is an international organization of individuals and companies concerned with or interested in Electrochemistry and allied subjects.

The Society is dedicated to the advancement of the theory and practice of Electrochemistry and related subjects, as shown in the following divisions:

Battery	Electro-Organic
Corrosion	Electrothermic
Electric Insulation	Industrial Electrolytic
Electrodeposition	Theoretical Electrochemistry
Electronics	

Among the means to this end are the holding of meetings for the reading and discussion of professional and scientific papers on these subjects, the publication of such papers, discussions, and communications as may seem appropriate, and cooperation with chemical, electrical, and other scientific and technical societies.

It is an incorporated society without capital stock. The affairs of the Society are managed by a Board of Directors under a Constitution and By-Laws. Officers are nominated by a nominating committee appointed by the Board of Directors and elected by the members.

Direct all general correspondence and inquiries regarding membership to Society headquarters at 235 West 102nd Street, New York 25, N. Y., c/o Mr. W. J. Holian, Assistant Secretary.

Officers of the Society

President ..... CHARLES L. FAUST
Past President ..... ALFRED L. FERGUSON
Vice-President ..... RALPH M. HUNTER
Vice-President ..... J. C. WARNER
Vice-President ..... ROBERT J. MCKAY
Treasurer ..... E. GIDEON WIDELL
Secretary ..... HENRY B. LINFORD

UMI